ASTRONOMY & ASTROPHYSICS
SUPPLEMENT SERIES

Astron. Astrophys. Suppl. Ser. **54**, 1-18 (1983)

Neutral hydrogen observations of double spiral galaxies. III. NGC 3504/3512, NGC 4085/4088, IC 65/UGC 622, NGC 797/801

G. A. van Moorsel

Kapteyn Astronomical Institute, Postbus 800, 9700 AV Groningen, The Netherlands

Received March 21, accepted May 10, 1983

Summary. — The four binary systems mentioned in the title of this paper have been observed in the 21 cm neutral hydrogen line with the WSRT. All 8 galaxies have been detected ; in the field of IC 65/UGC 622 two additional systems containing hydrogen were found. For these ten galaxies systemic velocities and rotation curves have been derived, and the total mass of each system has been determined in two ways : summing the results from the rotation curves, and calculating the minimum mass which follows from the orbital motion. In two of the four systems (NGC 3504/12 and IC 65/UGC 622) the minimum orbital mass is larger than the mass deduced from the rotation curves indicating the presence of invisible material.

Key words : HI observations — binary galaxies — redshifts.

1. Introduction.

This is the third paper in a series which describes observations of pairs of spiral galaxies and analyzes the results. The observations have been made using the Westerbork Synthesis Radio Telescope (WSRT). In the previous two papers (van Moorsel, 1982a (paper I) and 1983 (paper II)) five pairs have been presented and discussed. The aim of the project, a discussion of the observations, the reduction techniques, and the choice of the sample of objects to be observed were discussed extensively in a previous paper (van Moorsel, 1982a) ; consequently these points will be discussed briefly in the present paper.

For both members of each binary system the rotation curve and the systemic velocity are determined. The rotation curves furnish a measure of the total mass of each galaxy within the last measured point. The systemic velocities, on the other hand, give a lower limit to the total mass of the binary system. The two resulting mass values can be compared to see whether matter is present outside the region covered by HI.

In the present paper, the following pairs are presented :

i) NGC 3504 and NGC 3512 ;
ii) NGC 4085 and NGC 4088 ;
iii) IC 65 and UGC 622 ;
iv) NGC 797 and NGC 801.

The pair NGC 797/801 has been observed previously in the 21 cm line with the 91 m telescope at Green Bank (Peterson, 1979).

In section 2 we describe the photographic appearance of the four pairs. Section 3 briefly summarizes the observation and reduction techniques. In section 4 the results of the observations will be analyzed, and in section 5 these results will be discussed.

2. Description of the pairs.

NGC 3504/NGC 3512.

A reproduction from the blue Palomar Sky Survey print of the region surrounding this pair is shown in figure 1. A third system of unknown radial velocity is visible to the north-east, but it is considerably smaller in size ; if it is associated with the pair NGC 3504/3512, it probably does not noticeably interfere with the dynamics. In the vicinity of NGC 3504 and NGC 3512 a number of small, presumably background systems can also be seen.

A high quality photograph of NGC 3054, the westernmost of the two, is shown in the Hubble Atlas of Galaxies (Sandage, 1961), where it is classified as an Sb/SBb galaxy. The two spiral arms have a circular appearance suggesting that NGC 3504 may be oriented almost face-on. If, however, the bright main body is assumed to be circular in the plane of the galaxy the inclination is approximately 60° (Burbidge *et al.*, 1960), and the two spiral arms would have an elongated shape. Since a recent photograph of NGC 3504 (Sandage and Tamman, 1981) clearly shows the stellar nature and spiral structure of the bright central body, an inclination angle of 60° has been adopted in this paper.

NGC 3512 has been classified as Sc (Nilson, 1973). It is seen almost face-on, judging from the optical dimensions. In this paper an inclination of 20° will be used for NGC 3512.

The distance, using a Hubble constant of 100 km/s/Mpc, is 14.1 Mpc, and the angular separation is 12.′0, corresponding to 49 kpc.

NGC 4085/NGC 4088.

Figure 2 shows a reproduction from the blue Palomar Sky Survey print of the region around the binary system formed by NGC 4085 and NGC 4088. Both galaxies are

classified Sc (Nilson, 1973). In particular NGC 4088, the northernmost and brightest of the two, shows well developed spiral arms. The inclinations of NGC 4085 and NGC 4088, determined from the blue sizes in the Uppsala Catalogue and the axial ratios given in the Second Reference Catalogue (de Vaucouleurs, 1976) are 73° and 68°, respectively. The relatively high inclinations ensure a weak dependence of the derived rotational velocities on uncertainties in the inclinations. Adopting a Hubble constant of 100 km/s/Mpc, the distance to the pair is 8.3 Mpc. Their angular separation of 11.5 arcminutes corresponds to 28 kpc.

IC 65/UGC 622.

A reproduction from the blue Palomar Sky Survey print covering the region of observation around IC 65 and UGC 622 is shown in figure 3. The highly inclined system in the lower left corner is IC 65, classified as Sb/SBc. To the left of the bright star in the field, approximately 19 arcminutes to the north-west of IC 65 is UGC 622. This apparently small system does not show much structure in the photograph. It has been assigned type Sc (Nilson, 1973). To the north of the bright star, partly covered by it, a third, inconspicuous system can be seen. Because of its apparent high inclination this system will henceforward be referred to as « edge-on ». It has no entry in any existing catalogue. Fourteen minutes of arc due west of the bright star lies UGC 608. Its low surface brightness (m = 15.6) excluded it from consideration as a third member of the group formed by IC 65 and UGC 622. The centre of observation lies halfway between IC 65 and UGC 622. This means that UGC 608 is also included in the field of observation, although possible HI emission from it will be attenuated by about a factor of two due to primary beam effects. A close look of the field reveals the existence of several other, inconspicuous objects of extragalactic appearance. With H = 100 km/s/Mpc the distance to this group is 28.9 Mpc. The separation of IC 65 and UGC 622 (19.5 arcmin) corresponds to 164 kpc.

NGC 797/NGC 801.

Figure 4 shows the region of the sky around NGC 797 and NGC 801 (reproduction from the blue Palomar Sky Survey print). NGC 797 is the southern system, with the clearly developed spiral arms. This galaxy has type Sa/SBa (Nilson, 1973).

The northern system, NGC 801, is seen almost edge-on ; it has type Sc (Nilson, 1973). No other systems of comparable size are seen in the vicinity of this pair. The adopted distance to this pair is 58.9 Mpc (H = 100 km/s/Mpc). At that distance the angular separation of 9.1 minutes of arc corresponds to a linear separation of 156 kpc.

3. Observation and reduction.

The four fields were observed with the WSRT (Högbom and Brouw, 1974), using the digital line backend (DLB) (Bos *et al.*, 1981). Observational details of each individual observation are summarized in table I. After Fourier transformation of the data, the observations were analyzed using the « GIPSY » interactive image processing system (Shostak and Allen, 1979). The observations comprised 63 maps at different frequencies, each map having coordinates right ascension and declination.

Pure line channels were obtained by subtracting a continuum map, formed by averaging line-free channel maps. A global profile of each galaxy was used to derive a value for the total mass of neutral hydrogen in that galaxy, with usual assumptions of optically thin emission, and, for symmetric profiles, an accurate systemic velocity. By analyzing the velocity profile at each grid point in the sky coordinates plane the rotation curve could be constructed, and a separate determination of the systemic velocity was possible. The rotation curves serve as mass estimators of the individual galaxies, and the radial systemic velocity differences give a lower limit to the total mass of the binary system.

The mass of each galaxy given in table II was calculated from its rotation curve using the model and method developed by Nordsieck (1973). This method assumes that matter is distributed in a thin disk. The assumption of a spherical distribution gives masses which are up to 30 % higher than the thin disk masses (paper I) ; they follow directly from the outermost point on the rotation curve. The lower limit to the total mass of the binary system given in table III was calculated on the basis of two-body kinematics (paper I).

4. Results.

Data and results of the present observations are given in table II. In this section the results are briefly discussed ; for a more extensive treatment refer to van Moorsel (1982b).

NGC 3504/NGC 3512.

NGC 3504 has a strong central continuum source of 305 ± 8 mJy, shown in figure 5, which agrees well with a previous value of 310 mJy at 1420 MHz (Hummel, 1979). The central continuum source in NGC 3512, shown in figure 6, coincides with the optical central position (Dressel and Condon, 1976).

The low HI surface brightness made it necessary to convolve the channel maps to a 1′ × 1′ beam. In both galaxies therefore the smaller scale structure is sacrified in favour of the sensitivity for extended emission. In NGC 3504 (Fig. 8) the HI is concentrated towards the regions where the spiral arms originate from the central body ; in NGC 3512 (Fig. 9), where the HI extends beyond the optical boundaries, almost no structure is seen.

For both NGC 3504 and NGC 3512 the position-velocity plot method was used to obtain kinematical information (Fig. 11). For NGC 3504 the major axis position angle was determined from the HI centroids in the channel maps (Fig. 10), and for NGC 3512 this was done using the channel maps in figure 13 and the (heavily beam-smeared) velocity field in figure 14. Note that the major axis position angle of NGC 3504 as derived from kinematical data is consistent with the position angle from the optical picture assuming the central body is circular in shape.

The resulting rotation curves in figure 12 and 15 suffer badly from the large beam. Assuming that the rotation velocity at larger radii is approximately constant, the

outermost velocity and the total mass are not much affected. The actual extent is uncertain, however, but this uncertainty only enters linearly into the expression for the total mass.

NGC 4085/NGC 4088.

Figure 16 shows that in NGC 4085 the area with continuum emission occupies the central region of the optical disk, and that there is an indication of continuum emission *not* confined to the disk plane. NGC 4088 has continuum emission over the whole optical disk (Fig. 17), with a tendency of enhanced emission close to the spiral arms. The total flux density (235 ± 5 mJy) lies close to Hummel's (1979) 213 mJy at 1420 MHz.

The HI emission from NGC 4088 (Fig. 20) extends beyond the optical image. There is at least one clear HI ridge, probably associated with a spiral feature. Rotation curves were obtained by means of the position-velocity plot method for NGC 4085 (Fig. 21), and using the velocity field (Fig. 24) for NGC 4088. NGC 4085 is very symmetric ; in NGC 4088 there is a slight hint of a varying major axis position angle from the isovelocity contours, but not enough to claim the presence of mutual tidal interaction.

IC 65/UGC 622.

In addition to the additional pair members also UGC 608 and the unclassified edge-on system (see sects. 2, 3) were detected in HI. For IC 65 and UGC 622 smoothed data were used throughout, corresponding to a 40″ × 40″ beam. Each one of these four galaxies show asymmetric features in their HI distributions (Figs. 27-30), especially UGC 622. In addition, in the IC 65 field in the north-eastern corner, there is a barely significant HI detection coinciding with faint optical features. The presence of HI asymmetries and the small dispersion in radial velocities makes it likely that all detected galaxies are members of *one* group. Position-velocity plots of these galaxies (Figs. 31, 33, 35, and 37) were used to determine rotation curves. For the edge-on galaxy, this plot was also used to determine the central position, which is clearly not possible optically. This was done using symmetry arguments. The HI detection in the field of IC 65 has a systemic velocity of 2760 ± 10 km/s, and a width of 130 km/s, so that its mass may be comparable to that of the edge-on galaxy. Note that the rotation curves suffer from the large beam sizes.

NGC 797/NGC 801.

Both galaxies show weak associated continuum emission (Figs. 39 and 40). The situation in NGC 797 is reminiscent of the usual appearance of two-lobed radio galaxies. One of the detections, however, coincides with the map centre, which suggests that instrumental effects may be responsible for its existence, although the absence of this effect in other fields is a point in favour of its being real !

NGC 797 was barely detected in HI. On the basis of the profile obtained by Peterson (1979) a much stronger signal was expected, with an integrated emission equal to 12.8 Jy.km/s. Recent observations with the 100 m Effelsberg telescope at Bonn giving as upper limit 2.37 Jy.km/s (Richter, O. G. and Huchtmeyer, W. K., private communication) confirm the lack of HI in NGC 797. For NGC 797 all maps were convolved to a 45″ × 45″ beam ; for NGC 801 the original data were used. The HI emission in NGC 797 (Fig. 42) is seen to be not only weak, but asymmetric as well. Also in the case of NGC 801 the HI is concentrated towards one end of the galaxy (Fig. 43). The absence of HI in the northeastern part of NGC 797 greatly complicated the determination of the necessary parameters. The systemic velocity was estimated using a position-velocity plot along the *minor* axis (Fig. 44). Using this value, the rotation curve was obtained by means of the position-velocity plot along an axis close to the major axis, making use as efficiently as possible of the available HI information, and subsequently correcting the velocities for this offset in angle. Even after smoothing to a 100″ × 100″ beam and to twice the original velocity resolution the position-velocity plot along the major axis in figure 46 shows no significant HI detection in the northeastern part.

5. Discussion.

Table III summarizes all parameters relevant to the comparison between the sum of the individual masses, derived from the rotation curves, and the minimum orbital mass. The uncertainties given lie approximately at a 2 σ level ; note the high uncertainties in the case of low-inclination galaxies.

The parameter $\chi_{obs} \equiv M_{orb}/\Sigma m_i$ in column 7, which is independent of the adopted Hubble constant, is suitable to characterize the amounts of undetected mass. If *no* dark matter is present, $\chi_{obs} \equiv \chi$, where χ is the ratio of M_{orb} and the (unknown) total amount of mass in the orbit. Adopting the two-body model, the parameter χ is a function of orbital orientation angles only, and has a known probability distribution function assuming random orbital orientation and phases. This distribution is non-zero between $\chi = 0$ and $\chi = 1 + e$, e being the orbital eccentricity, and is strongly peaked toward $\chi = 0$. By comparing the *theoretical* distribution of χ and the *observed* distribution of χ_{obs} for a large number of pairs, it is possible to draw solid conclusions about the existence of dark matter in binary systems. Generally speaking, a χ_{obs} exceeding unity is a strong indication for the presence of dark matter. More details about these parameters and their significance is given in van Moorsel, 1982b, chapter 8.

NGC 3504/NGC 3512.

This pair has a χ_{obs} value which is definitely larger than the « theoretical » maximum $\chi_{obs} = 1$ for circular orbits and an order of magnitude larger than the expectation value $\chi_{obs} = 0.3$ (paper I). One of the possibilities is that the rotation curve extends much farther out than is actually observed. The pair must then essentially be a « contact-binary » seen at a favourable viewing angle. A second possibility would be that the two components of the pair move in a common extended massive halo ; in that case the observed radial velocities are not a measure of the total mass between the galaxies. This discrepancy between the sum of the individual masses and the minimum orbital mass occurs for several pairs in this study, and will be discussed in more detail in a later paper.

NGC 4085/NGC 4088.

The value of χ_{obs} for this binary system is consistent with a picture in which the plane of the orbital motion is oriented face-on with respect to the observer, so that the projected radial velocity difference will always be close to zero.

IC 65/UGC 622.

This pairs has $\chi_{obs} > 1$ in common with the pair NGC 3504/3512, but an additional problem is caused by the presence of UGC 608, which has a total mass comparable to that of UGC 622, and the edge-on system, which has a mass roughly a factor 3 lower. For reasons of consistency with the other pairs, IC 65 and UGC 622 are treated as a *pair* in table III. In van Moorsel, 1982b, chapter 9, it is shown that for groups consisting of N galaxies a projection function χ_N can be defined, which may directly be compared with the χ for the case of a binary system. If the present four galaxies are treated as one group, a χ_4 value of 2.3 results. Although this means that the original value of χ_{obs} is lowered, it is not sufficient at all to reject the possible presence of dark matter in the quadruple system. A similar situation applies to the pair NGC 5673/IC 1029 (van Moorsel, 1983).

NGC 797/NGC 801.

The χ_{obs} value for this binary system is consistent with the value expected for two point masses moving in an elliptic orbit, with the masses given by the rotation curves. The error in χ_{obs} could be greatly reduced by a new observation of NGC 797 with the WSRT, which has been considerably improved in sensitivity since the observations were made.

Combining the results from the previously observed five binaries (papers I and II) with the present results, it is striking that four out of the nine binaries have χ values far exceeding the theoretical limit of 1. An extensive discussion on this phenomenon will be made after the results of five other binaries, to appear in a next paper, are known. For the moment the two most probable explanations are :

i) because of the presence of dark matter the two-body model is not directly applicable in cases where $\chi_{obs} > 1$.

ii) In cases where $\chi_{obs} > 1$, the two galaxies are in an hyperbolic orbit, and their velocity difference consequently is not caused by the gravitational potential alone.

Acknowledgments.

I would like to thank the staff of the Netherlands Foundation for Radio Astronomy for their assistance during and after the observations, G. Comello for the many drawings, W. Haaima for the photography, and the secretarial staff at the Kapteyn Institute for the typing. I am grateful to T. S. van Albada, R. Sancisi, and G. S. Shostak for their advice during the present project, and for their critical reading of the manuscript, and to Z. W. O. for financial support.

The Westerbork Synthesis Radio Telescope is operated by the Netherlands Foundation for Radio Astronomy which is financially supported by the Netherlands Organization for the Advancement of Pure Research (Z.W.O.).

References

Bos, A., Raimond, E. and Someren Greve, H. W. van : 1981, *Astron. Astrophys.* **98,** 251.
Burbidge, E. M., Burbidge, G. R., Prendergast, K. H. : 1960, *Astrophys. J.* **132,** 661.
Dickel, J. R. and Rood, H. J. : 1978, *Astrophys. J.* **223,** 391.
Dressel, L. L. and Condon, J. J. : 1976, *Astrophys. J. Suppl. Ser.* **31,** 187.
Högbom, J. A. and Brouw, W. N. : 1974, *Astron. Astrophys.* **33,** 289.
Hummel, E. : 1980, *Astron. Astrophys. Suppl. Ser.* **41,** 151.
Moorsel, G. A. van : 1982a, *Astron. Astrophys.* **107,** 66 (paper I).
Moorsel, G. A. van : 1982b, Ph. D. Thesis, University of Groningen.
Moorsel, G. A. van : 1983, *Astron. Astrophys. Suppl. Ser.* **53,** 271 (paper II).
Nilson, P. : 1973, Uppsala General Catalogue of Galaxies, *Uppsala Astron. Obs. Ann.,* 6.
Nordsieck, K. H. : 1973, *Astrophys. J.* **184,** 719.
Peterson, S. : 1979, *Astrophys. J.* **232,** 20.
Sancisi, R. and Allen, R. J. : 1979, *Astron. Astrophys.* **74,** 73.
Sandage, A. : 1961, *Hubble Atlas of Galaxies* (Carnegie Institution of Washington Pub.) n° 618.
Sandage, A. and Tamman, G. A. : 1981, *A Revised Shapley-Ames Catalog of Bright Galaxies* (Carnegie Institution of Washington Publ.) n° 635.
Shostak, G. S. and Allen, R. J. : 1979, *in ESO Workshop on Two Dimensional Photometry,* P. Crane and K. Kjär (Noordwijkerhout).
Vaucouleurs, G. de, Vaucouleurs, A. de, Corwin, H. G. : 1976, *Second Reference Catalogue of Bright Galaxies* (University of Texas Press, Austin).
Warner, P. J., Wright, M. C. H., Baldwin, J. E. : 1973, *Mon. Not. R. Astron. Soc.* **163,** 163.
Zwicky, F., Herzog, E., Karpowicz, M., Kowal, C. T., Wild, P. : 1961-1968, *Catalogue of Galaxies and of Clusters of Galaxies,* vols. 1-6 (Pasadena, California Institute of Technology).

TABLE I. — *Parameters of the observations.*

	NGC 3504/NGC 3512	NGC 4085/NGC 4088	IC 65/UGC 622	NGC 797/NGC 801
date of observation	February 1979	July 1979	July 1979	August 1978
length of observation (hours)	12	12	12	12
number of interferometers	40	36	36	40
baselines (m) (smallest, largest, increment)	36-1440-36	36-1296-36	36-1296-36	36-1440-36
synthesized beam (sec. of arc)	25 × 53	27 × 35	27 × 36	25 × 41
radii first grating ring (min. of arc)	20.3 × 42.9	20.3 × 26.2	20.3 × 27.5	20.3 × 33.1
FWHP primary beam (min. of arc)	37.6	37.6	37.6	37.6
rms noise channel maps (K)	1.3	1.6	1.9	1.6
velocity central channel (km/s), heliocentric	1465	700	2500	5700
bandwidth (MHz)	5	5	5	5
number of frequency channels	63	63	63	63
channel separation (km/s)	16.6	16.6	16.8	17.1
velocity resolution (km/s)	33	33	34	34
R.A. field centre (1950) (h, m, s)	11 00 54.0	12 02 54.0	00 57 48.0	02 00 24.0
Dec. field centre (1950) (°, ', ")	28 16 00	50 43 00	47 33 00	37 53 00
mJy-K conversion, equivalent of 1.0 K (mJy/beam area)	1.6(original maps) 5.6(smoothed maps)	1.2	1.1(original maps) 2.3(smoothed maps)	1.2(original maps) 3.3(smoothed maps)

TABLE II. — *Data and results.*

1-	3504	3512	4085	4088	I65	-	edge-on	-	797	801
2-	6118	6128	7075	7081	625	622	-	608	1541	1550
3-	Sa-SBb	Sc	Sc	Sc	Sb-SBc	Sb	Sbc?	SABdm	Sa-SBa	Sc
4-	11.5	12.9	12.8	11.2	13.8	14.6	?	15.6	13.1	13.5
5-	11 00 28.1	11 01 19.7	12 02 50.5	12 03 03.1	00 58 03.2	00 57 36.0*	00 57 08.3*	00 56 09.2*	02 00 27.9	02 00 44.9
6-	28 14 35	28 18 30	50 37 56	50 49 13	47 24 43	47 43 39*	47 46 17*	47 44 57*	37 52 41	38 01 11
7-	-	12.0	-	11.5	-	19.5	23.5	27.9	-	9.1
8-	60	20	76	69	77	52	90	66	44	86
9-	2.5	1.7	2.7	5.9	4.4	1.1	?	2.0	1.9	3.3
10-	3.1	2.7	2.8	5.8	4.1	1.7	?	2.5	2.7	3.0
11-	3.1	3.1	3.9	9.3	6.9	3.2	2.1	3.0	2.3	4.9
12-	1543 ± 5	1376 ± 5	752 ± 4	760 ± 4	2614 ± 4	2711 ± 8	2598 ± 8	2753 ± 4	5666 ± 15	5762 ± 5
13-	14.1		8.3		28.9				58.9	
14-	3.2	9.8	48	256	40.8	9.0	4.1	12.7	3.2	13.2
15-	1.5	4.6	7.8	41.6	80.2	17.7	8.2	24.9	26	108
16-	110	257	145	178	168	154	62	104	266	226
17-	1.0 ± 0.2	5 ± 3	1.3 ± 0.2	6.0 ± 0.8	9.8 ± 1.0	2.6 ± 0.6	0.6 ± 0.1	1.5 ± 0.3	40 ± 12	28 ± 2
18-	305 ± 8	6.5 ± 1.0	53 ± 3	235 ± 5	< 4.7	< 5.0	< 6.2	< 9.1	12 ± 2	16 ± 1
19-	155	140	78	43	153	145	170	125	65	149

* - positions are from this paper, estimated errors 0.5 sec in R.A., 5" in Dec.

Notes to table II.

1. NGC number or — if preceded by I — IC number.
2. UGC number.
3. Morphological type (from the UGC, Nilson, 1973).
4. Apparent photographical magnitude (from the CGCG, Zwicky *et al.*, 1961-1968).
5. Right Ascension of galaxy centre (1950.00) in h, m, s. From Dressel and Condon (1976), or using a central continuum source.
6. Declination of galaxy centre (1950.00) in °, ', ". From Dressel and Condon (1976), or using a central continuum source.
7. Distance to first galaxy in the pair (arcmin).
8. Inclination angle of plane of galaxy (°). From the UGC (Nilson, 1973), and the Second Reference Catalogue (de Vaucouleurs *et al.*, 1976).
9. Blue diameter in arcmin (Nilson, 1973).
10. Holmberg diameter in arcmin. Due to lack of photometry on these galaxies the empirical relation

$$d_H = 1.75 \cdot a^{0.84} \cdot (b/a)^{0.3}$$

is used (Dickel and Rood, 1978). Here a is the blue diameter (see 9), b the minor axis diameter, and d_H the empirically determined Holmberg diameter.

11. Largest extent of HI (arcmin), using the 2×10^{20} atoms/cm contour.
12. Systemic velocity (km/s) as determined in this paper.
13. Distance in Mpc using the mean radial velocity corrected by 300 sin l cos b (l and b are galactic coordinates), and a Hubble constant of 100 km/s/Mpc.
14. Total HI emission (Jy/km/s).
15. Total HI mass in units of $10^8 M_\odot$.
16. Maximum rotation velocity (km/s).
17. Total mass in units of $10^{10} M_\odot$.
18. Continuum flux (mJy). An upper limit gives the 3 σ noise level in mJy/beam area.
19. Position angle of the major axis, measured from north eastward.

TABLE III. — *Summary of results.*

1 NGC	2 UGC	3 radius (kpc)	4 m (10^{10} $M_\odot$)	5 Δv (km/s)	6 M_{orb} (10^{10} $M_\odot$)	7 $M_{orb}/\Sigma m_i$
3504	6118	5	6 ± 3	167 ± 7	32 ± 3	5.3 ± 2.9
3512	6128	5				
4085	7075	4	7.3 ± 0.8	8 ± 6	< 0.07	< 0.01
4088	7081	11				
IC65	625	21	12.4 ± 1.2	97 ± 9	36 ± 6	2.9 ± 0.8
-	622	8				
797	1541	40	68 ± 14	96 ± 16	33 ± 11	0.5 ± 0.3
801	1550	37				

Notes to table III.

Column Note

3 Distance from centre to outermost point on the rotation curve.

4 Sum of rotation curve masses. The error includes uncertainties in the inclination angle, but not effects of a different mass distribution (e.g. spherical rather than a flat disk).

5 Difference in radial velocities as given in table II.

6 Minimum orbital mass, calculated as

$$M_{orb} = 6.7 \times 10^4 (\Delta v)^2 \, . \, \Delta R \, . \, D \, ,$$

with Δv, ΔR, and D given in column 5 and table II.

7 Ratio of minimum orbital mass in column 6 and the sum of the individual masses in column 4. (χ_{obs}).

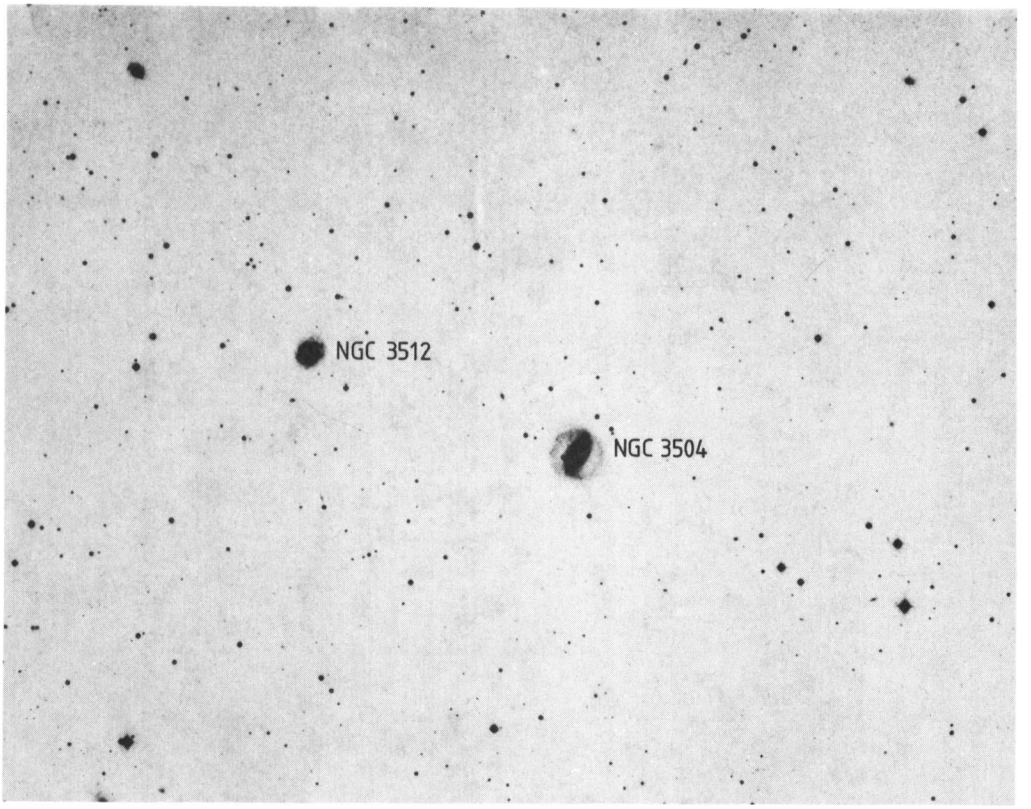

FIGURE 1. — A reproduction from the blue Palomar Sky Survey print showing NGC 3504 (west), and NGC 3512 (east). North is upward.

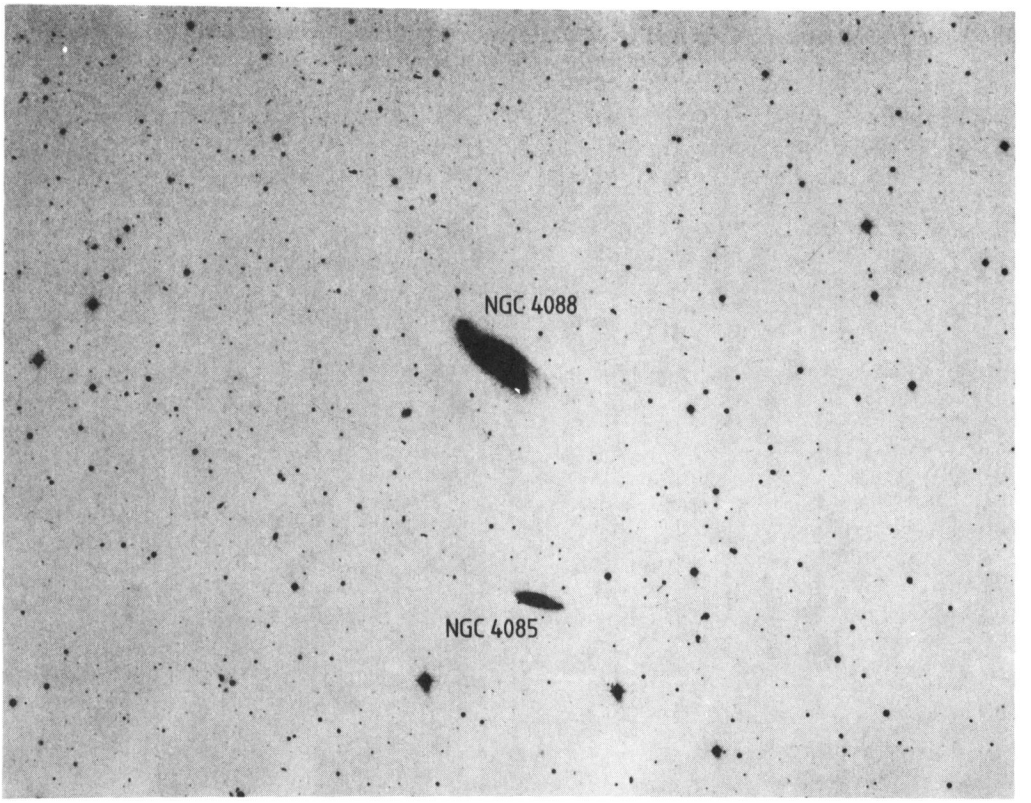

FIGURE 2. — The region of the sky around the binary system NGC 4085 (south), and NGC 4088 (north). East is to the left. Reproduction from the blue Palomar Sky Survey print.

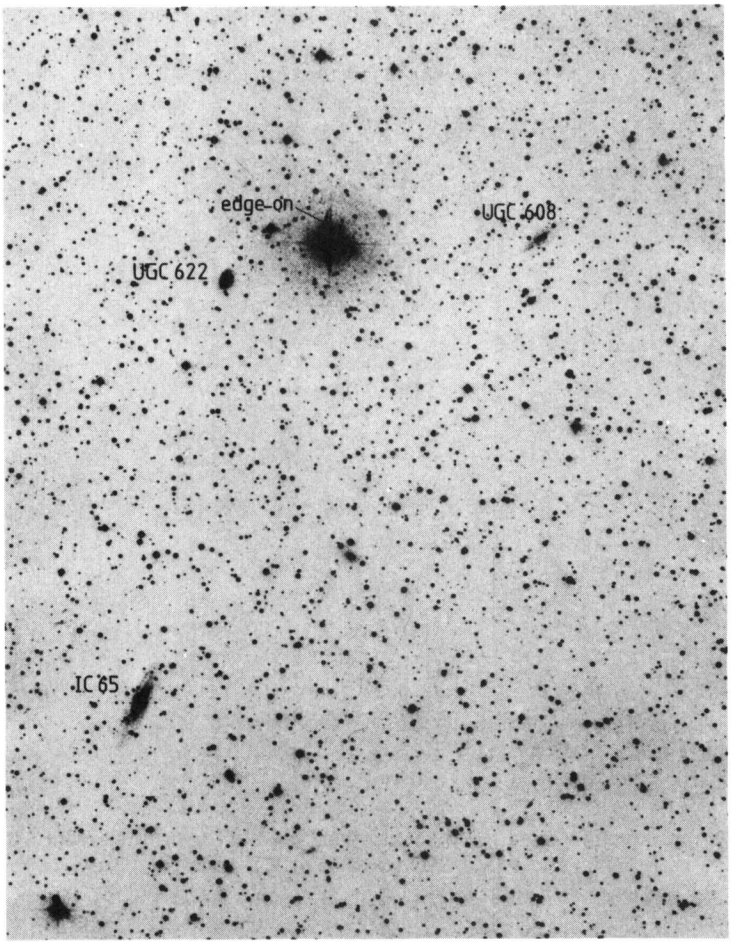

FIGURE 3. — The region around IC 65 and UGC 622 on a reproduction from the blue Palomar Sky Survey print. North is upward, east is to the left.

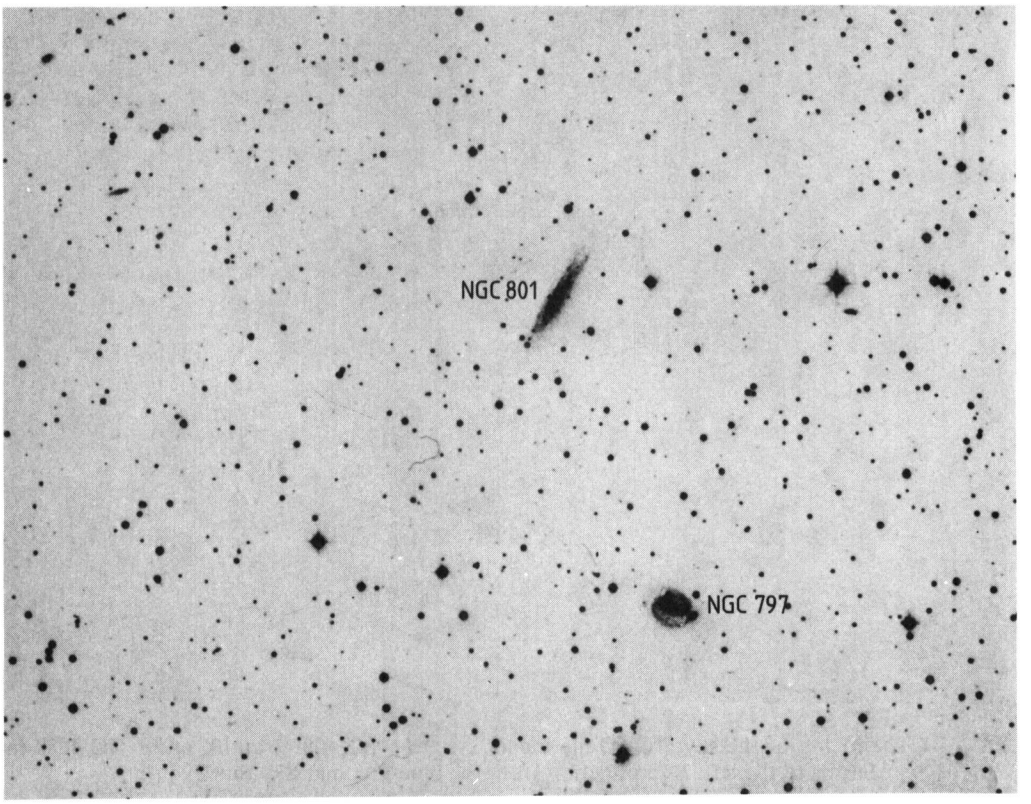

FIGURE 4. — A reproduction from the blue Palomar Sky Survey print showing NGC 797 (south), and NGC 801 (north). East is to the left.

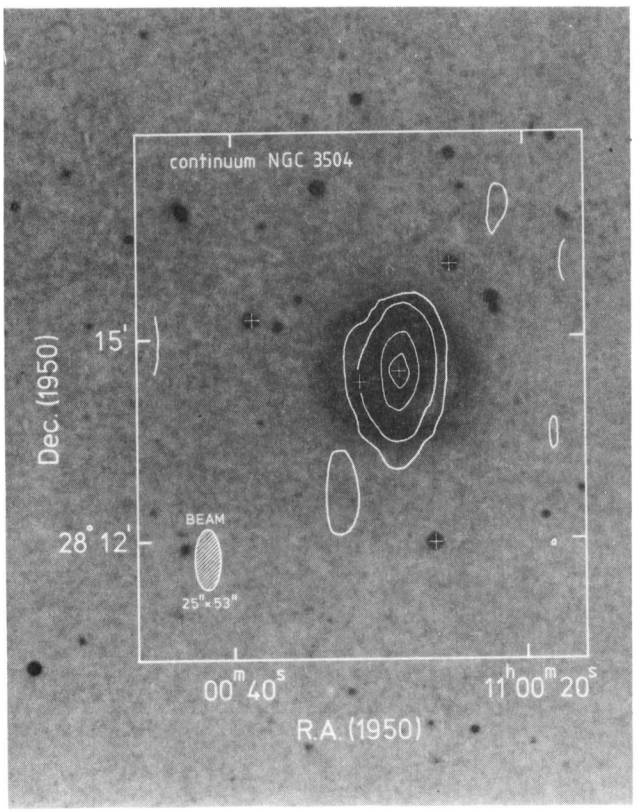

FIGURE 5. — Continuum map of NGC 3504. Contours shown are 2, 10, 70 and 140 mJy/beam area. The lowest contour corresponds to a 3 σ noise level. A primary beam correction has been applied.

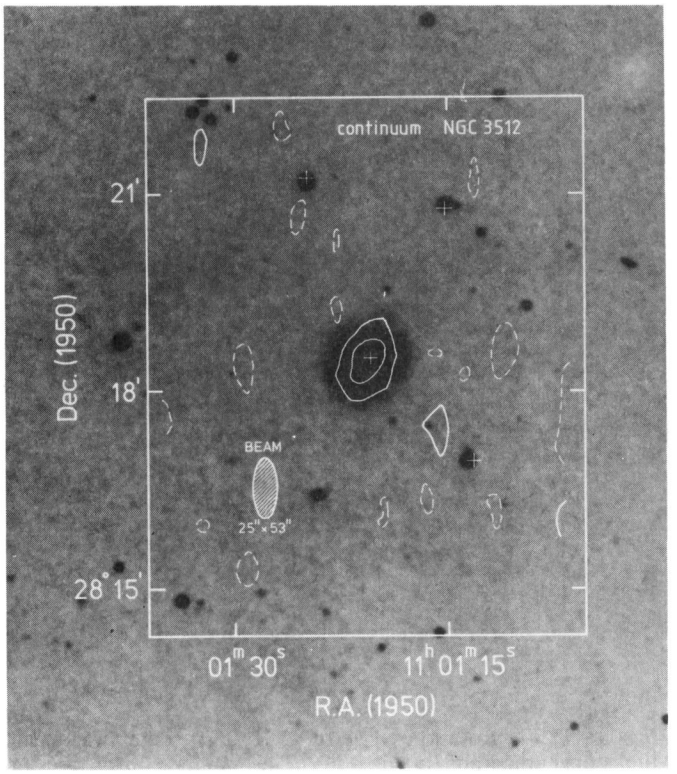

FIGURE 6. — Continuum map of NGC 3512, corrected for primary beam effects. Contours are − 1.25, 1.25 and 2.5 mJy/beam area. The negative contour is shown dashed ; 1.25 mJy corresponds to a 2 σ noise level.

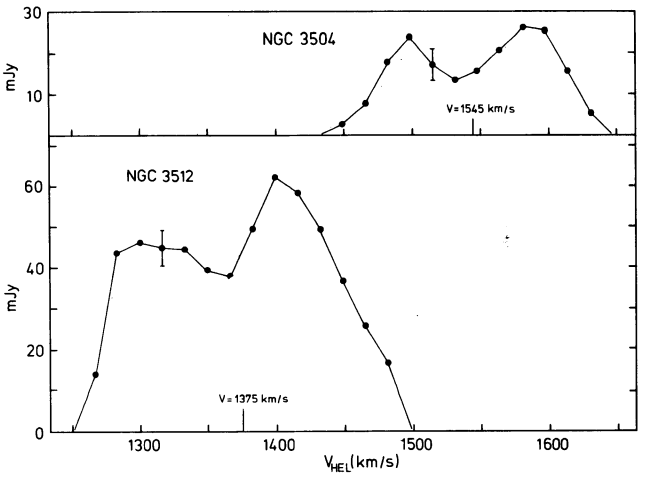

FIGURE 7. — Global profiles of NGC 3504 and NGC 3512. The indicated error bar is typical for the points in the profile. Systemic velocities determined from these profiles have been indicated.

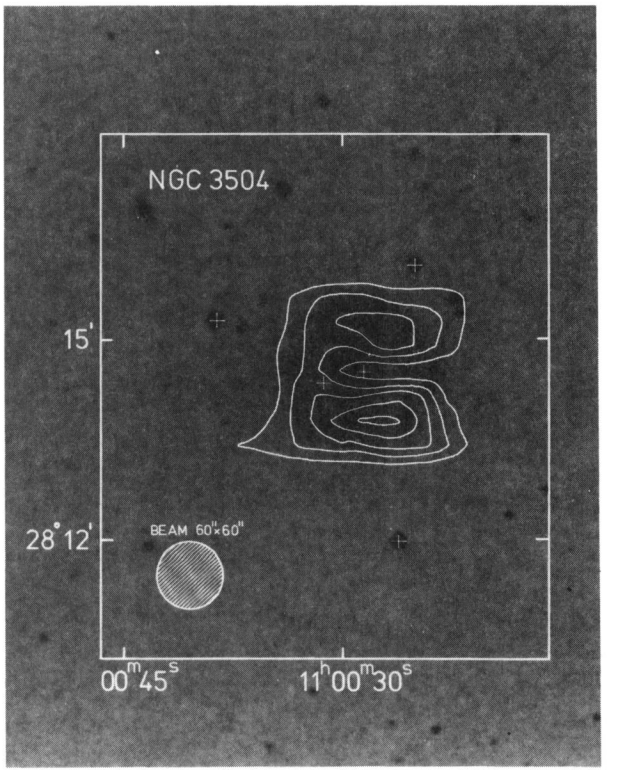

FIGURE 8. — Distribution of HI in NGC 3504 on a reproduction from a blue Palomar Sky Survey print. The map has been corrected for primary beam effects. The central cross marks the position of the continuum source. Contours are 1.1, 2.2, 3.3, 4.4 and 5.5 × 10^{20} atoms/cm^2. The lowest contour corresponds to a 3 σ noise level.

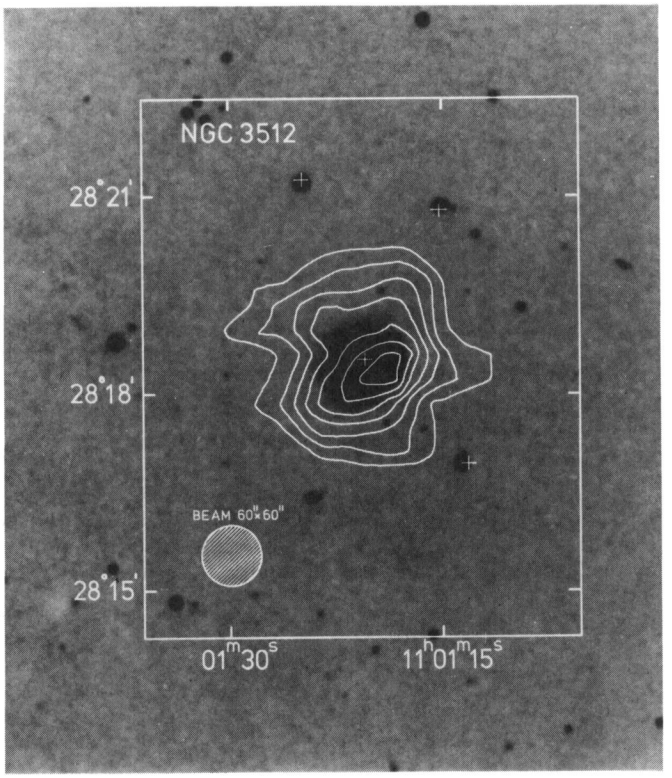

FIGURE 9. — Distribution of HI in NGC 3512 on a reproduction from a blue Palomar Sky Survey print. The map has been corrected for primary beam effects. The central cross marks the position of the continuum source. Contours are 1.1, 2.2, 3.3, 4.4 and 5.5, 6.6 and 7.7 × 10^{20} atoms/cm^2. The lowest contour corresponds to a 3 σ noise level.

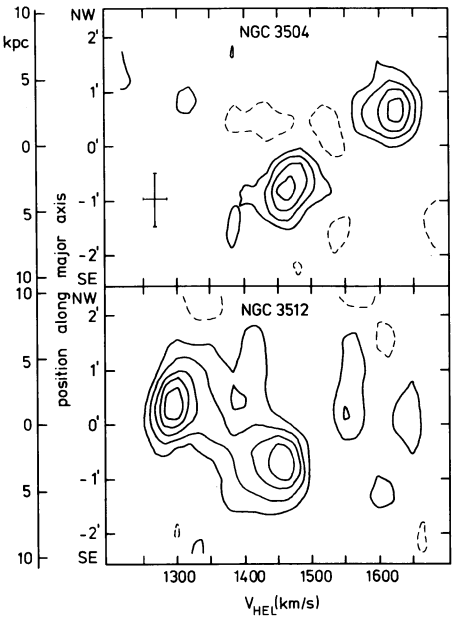

FIGURE 11. — Position-velocity plots of NGC 3504 and NGC 3512 on a common velocity axis. The resolution in velocity and space has been indicated by the cross in the upper diagram. Contours are − 0.7 K (dashed), 0.7 K (1.6 σ), 1.4 K, 2.1 K, 2.8 K and 3.5 K brightness temperature. The position angles of the major axes are 155° for NGC 3504 and 140° for NGC 3512.

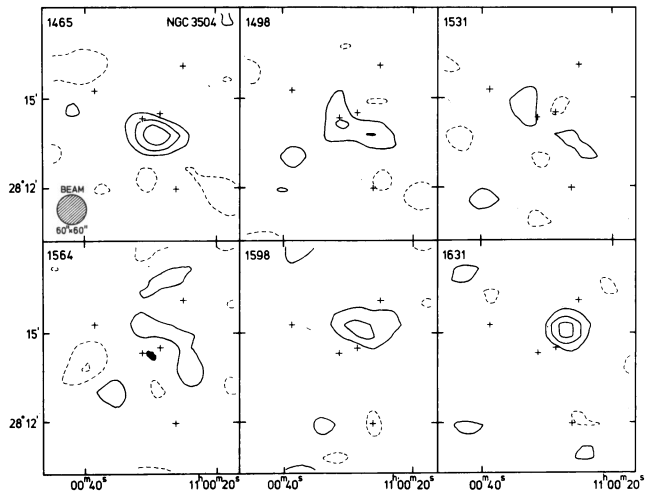

FIGURE 10. — Channel maps of NGC 3504. The corresponding heliocentric radial velocity is shown in the upper left hand corner of each map. The crosses are the same as in figs. 5 and 8. Contours are − 0.9 K (dashed), 0.9 K (2 σ noise level), 1.8 K and 2.7 K brightness temperature.

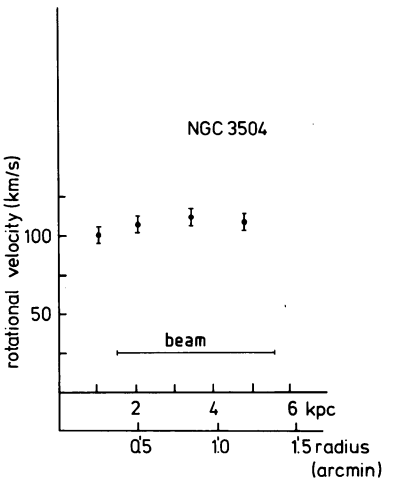

FIGURE 12. — Rotation curve of NGC 3504, determined from the upper diagram in fig. 11. The points shown are not independent, the height has been corrected for the inclination. The error bars do not include uncertainties in the inclination angle of NGC 3504.

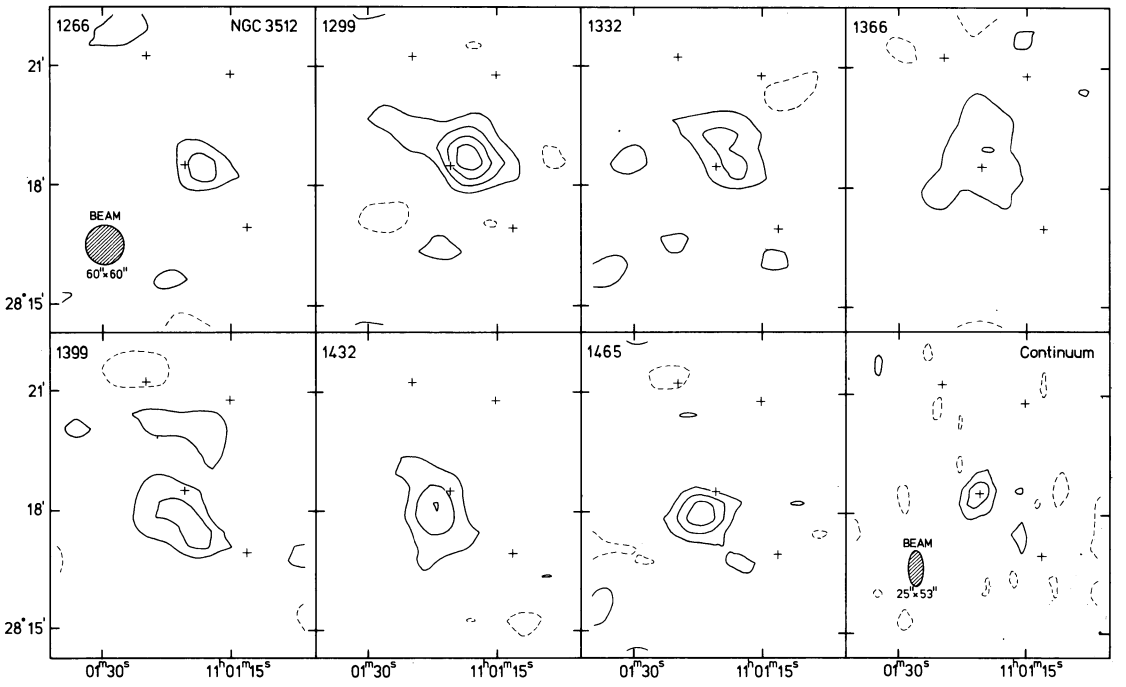

FIGURE 13. — Channel maps of NGC 3512, with the heliocentric radial velocity indicated in each panel. The crosses are the same as in figs. 6 and 9. Contours are − 0.9 K (dashed), 0.9 K (2 σ noise level), 1.8 K, 2.7 K and 3.6 K brightness temperature.

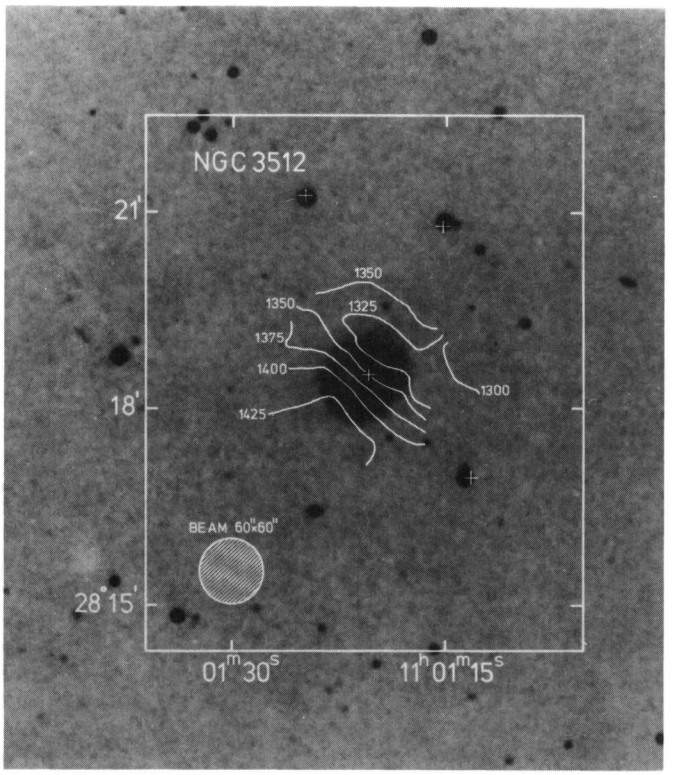

FIGURE 14. — Velocity field of NGC 3512. Heliocentric radial velocities are indicated. This velocity field is heavily affected by beam-smearing.

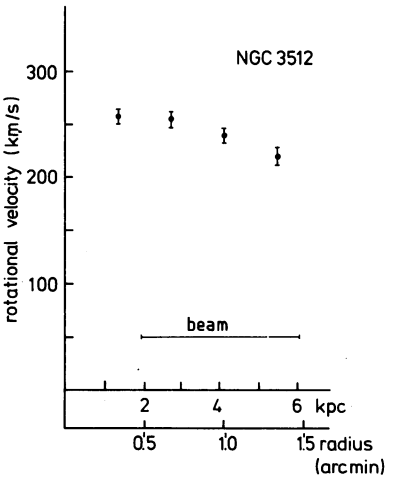

FIGURE 15. — Rotation curve of NGC 3512, determined from the lower diagram in fig. 11. The points shown are not independent ; the rotational velocities have been corrected for inclination. The error bars do not include uncertainties in the inclination angle of NGC 3504.

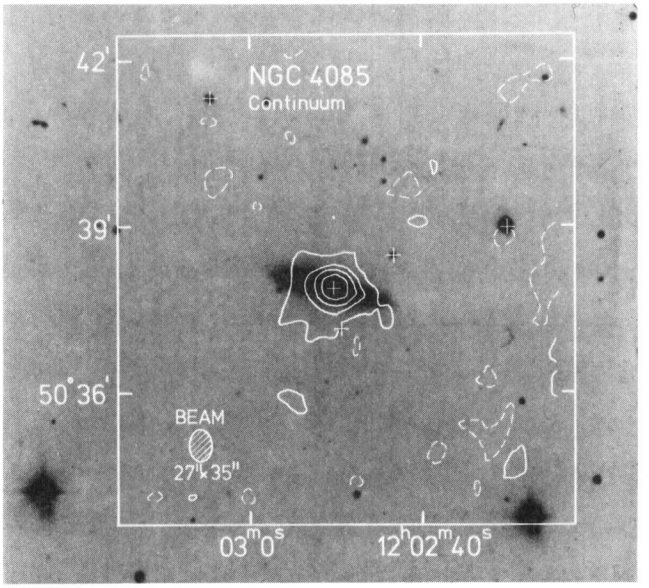

FIGURE 16. — Continuum map of NGC 4085, corrected for primary beam effects. The centroid of the continuum emission is indicated by the cross. Contours are − 1.8, 1.8, 3.6, 5.4 and 9.0 mJy/beam area. The negative contour is shown dashed ; the lowest positive contour corresponds to a 2 σ noise level.

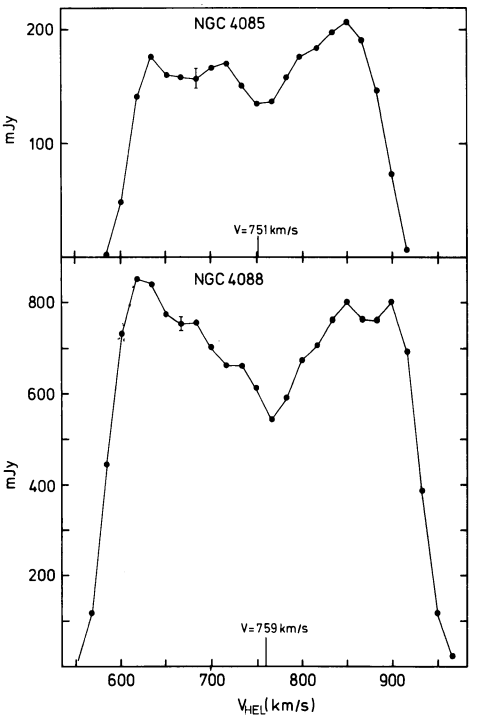

FIGURE 18. — Global profiles of NGC 4085 and NGC 4088, with typical uncertainties indicated by the error bar. Systemic velocities from these profiles are also included. The values shown have been corrected for primary beam attenuation.

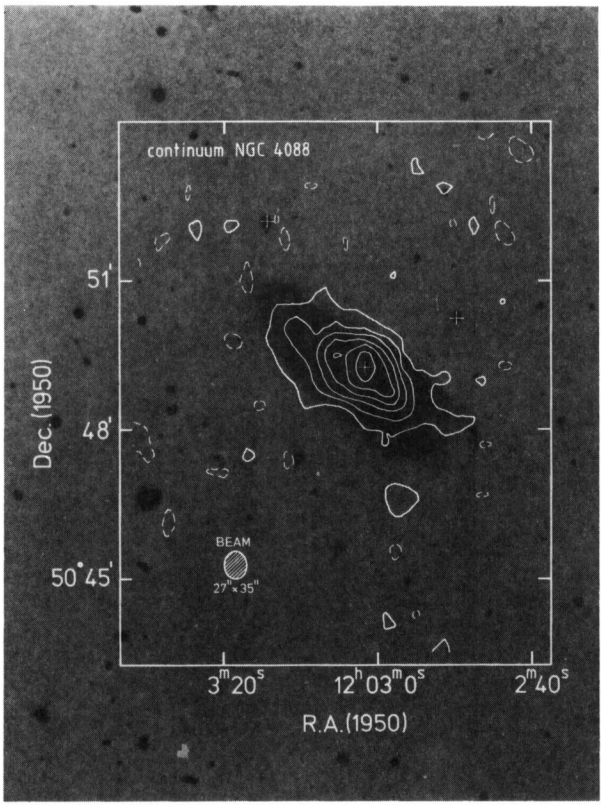

FIGURE 17. — Continuum map of NGC 4088, corrected for primary beam effects. The central cross indicates the centroid of the continuum emission. Contours are − 1.9 (dashed), 1.9 (2 σ noise level), 5.6, 9.4, 13.1, 16.9 and 20.6 mJy/beam area.

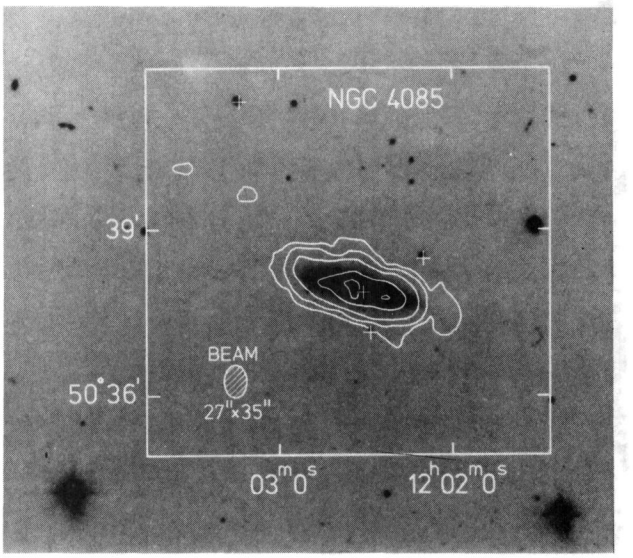

FIGURE 19. — Distribution of HI in NGC 4085. Contours are 3.7 (2.5 σ noise level), 7.4, 14.8, 29.7 and 44.5 × 10^{20} atoms/cm^2. The map has been corrected for primary beam attenuation.

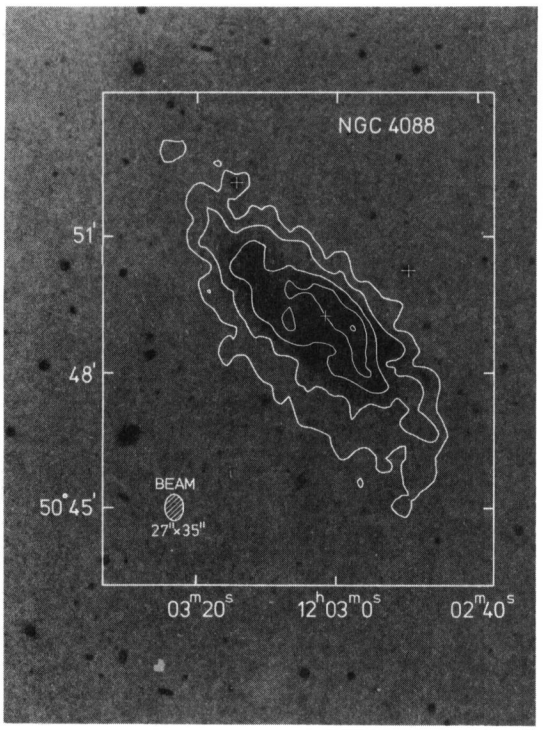

FIGURE 20. — HI distribution in NGC 4088, corrected for primary beam attenuation. Contours are 3.7 (2.5 σ noise level), 11.1, 22.2, 33.4, and 44.5 × 10^{20} atoms/cm^2.

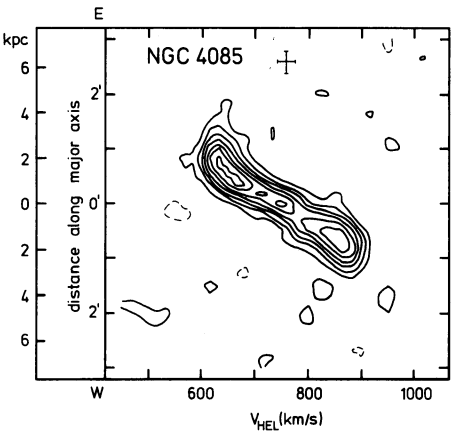

FIGURE 21. — Position-velocity plot of NGC 4085 along its major axis (position angle 78°). The cross indicates the resolution in velocity and in space (along the major axis). Contours are − 3.3 (dashed), 3.3 (2 σ noise level), 6.6, 9.9, 13.2, 16.5, 19.8 and 23.1 K brightness temperature.

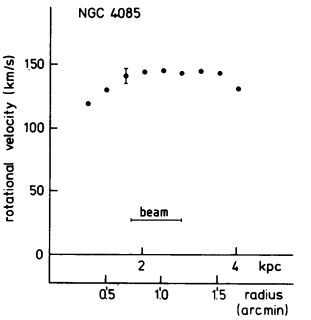

FIGURE 22. — Rotation curve of NGC 4085, as determined from fig. 21. Rotational velocities have been corrected for inclination.

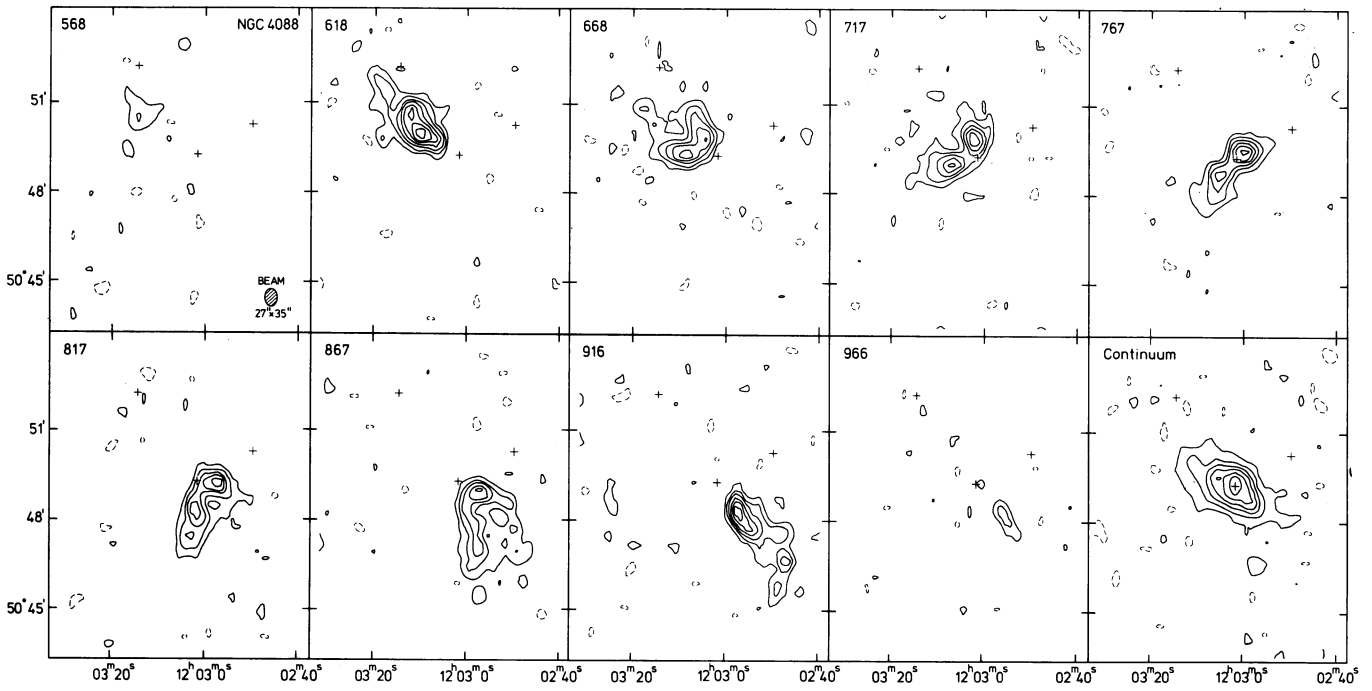

FIGURE 23. — Nine channel maps of NGC 4088. The heliocentric radial velocity is shown in the upper left hand corner of each channel map. Contours are − 3.7 (dashed), 3.7, 11.1, 14.8, 18.5, 22.2, and 25.9 K brightness temperature. The lowest contour lies on a 2 σ noise level. The crosses are the same as in figs. 17 and 20.

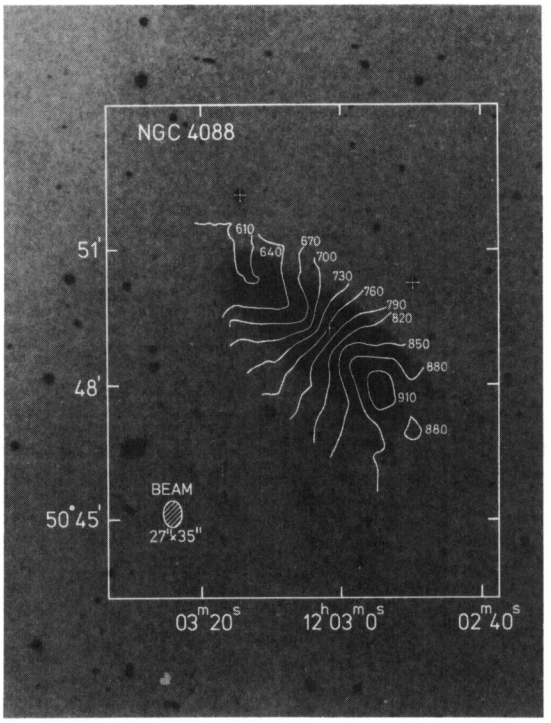

FIGURE 24. — Velocity field of NGC 4088. The contours are labelled with their corresponding heliocentric velocity. Contour « 760 » indicates the adopted systemic velocity of NGC 4088.

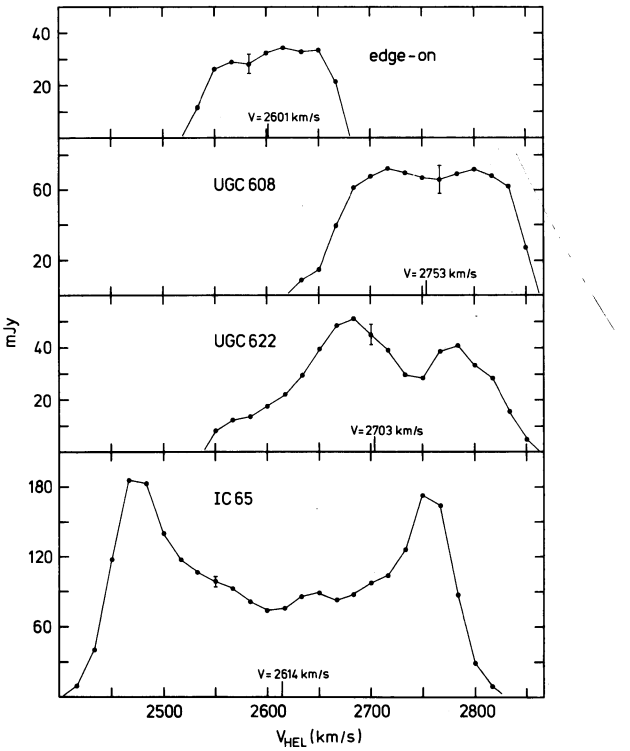

FIGURE 26. — Global profiles of IC 65, UGC 622, the « edge-on » system, and UGC 608 on a common velocity axis. Typical uncertainties and the derived systemic velocities are indicated. All flux densities shown have been corrected for effects of primary beam attenuation.

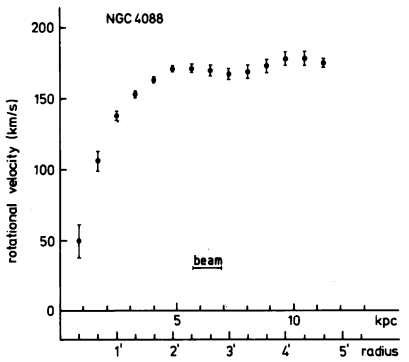

FIGURE 25. — Rotation curve of NGC 4088 determined from the velocity field in fig. 24. Rotational velocities have been corrected for inclination.

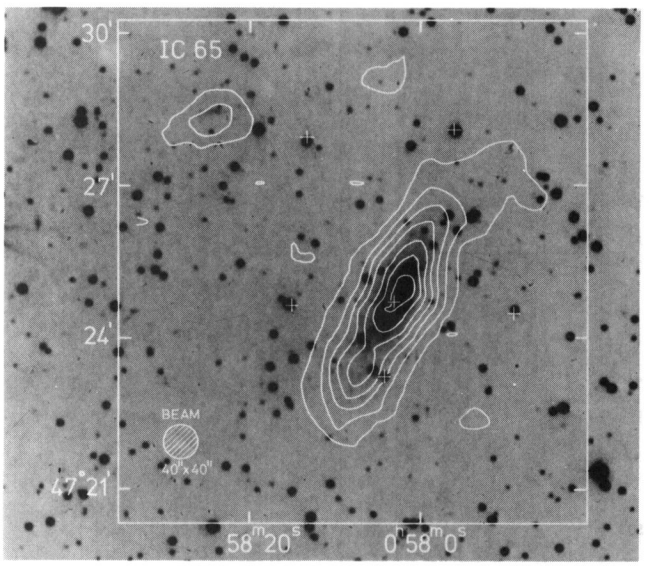

FIGURE 27. — The HI distribution of IC 65, corrected for primary beam attenuation. The central cross marks the optical centre. Contours are 2.3 (2.5 σ noise level), 6.8, 11.4, 15.9, 20.5, 25.0 and 29.6 $\times$ 10^{20} atoms/cm^2.

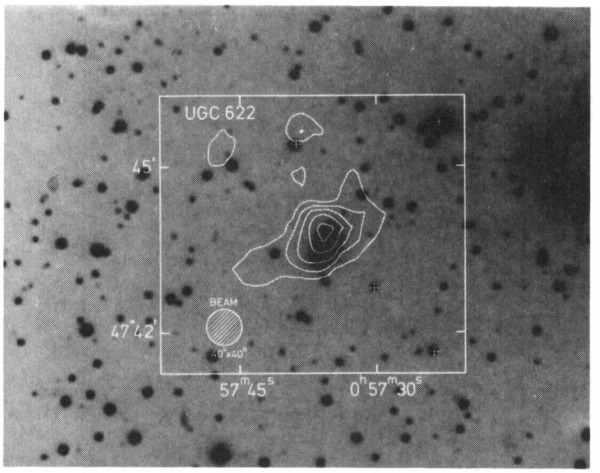

FIGURE 28. — The HI distribution of UGC 622, corrected for primary beam attenuation. Contours are 3.1 (3 σ noise level), 6.2, 9.3, 12.4 and 15.5 $\times$ 10^{20} atoms/cm^2.

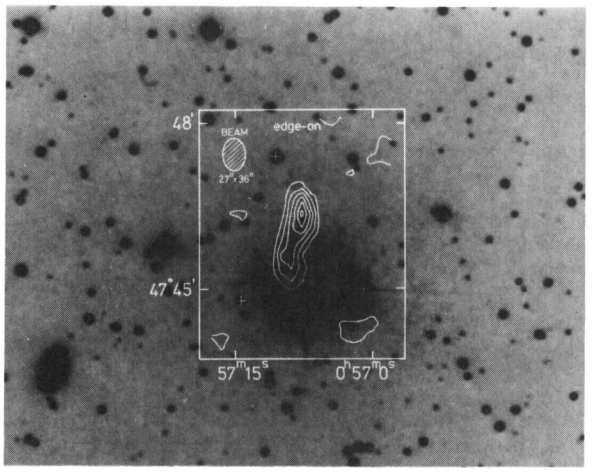

FIGURE 29. — The distribution of HI, corrected for primary beam effects, in the edge-on system. Contours are 5.3 (3 σ), 10.5, 15.8, 21.1, 26.4 and 31.6 $\times$ 10^{20} atoms/cm^2.

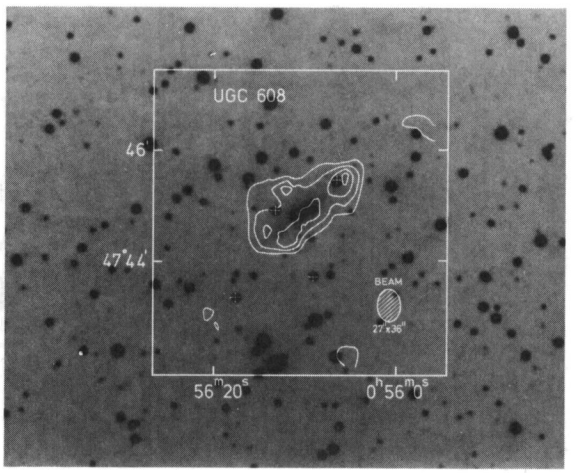

FIGURE 30. — HI distribution associated with UGC 608. The maps have been corrected for primary beam attenuation. Contours are 8.6 (2-2.5 σ), 17.1, 25.7, and 34.3 $\times$ 10^{20} atoms/cm^2. The high value of the lowest contour is caused by the large primary beam correction.

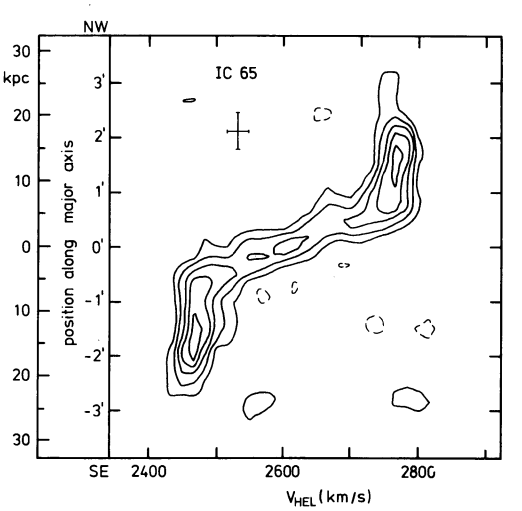

FIGURE 31. — Position-velocity plot along the major axis of IC 65 (position angle 153°). The cross indicates the resolution in velocity and in space. Contours are – 2.2 (dashed), 2.2 (2 σ noise level), 4.4, 6.6, 8.8 and 11.0 K brightness temperature.

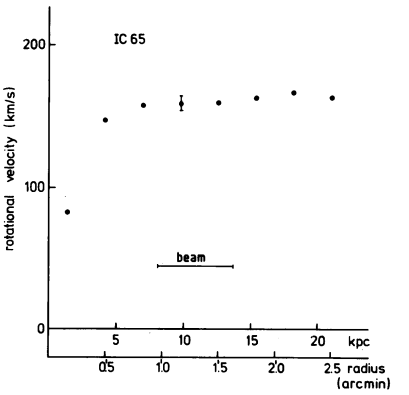

FIGURE 32. — Rotation curve of IC 65, determined from fig. 31, and corrected for an inclination of 77°. A typical uncertainty is indicated by the error bar.

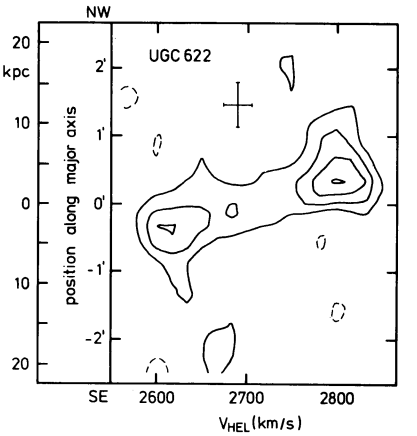

FIGURE 33. — Position-velocity plot along the major axis of UGC 622 (position angle 145°). The resolution in velocity and in space is indicated by the cross. Contours are – 3.0 (dashed), 3.0, 6.1, 9.1 and 12.2 K brightness temperature. The lowest contour corresponds to a 1.5 σ noise level.

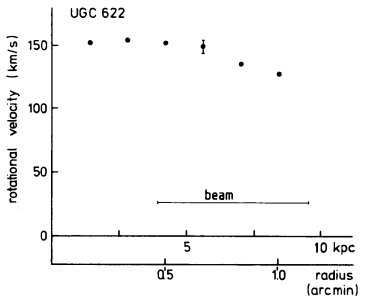

FIGURE 34. — Rotation curve of UGC 622, determined from fig. 33. Rotation velocities have been corrected for 52° inclination. A typical uncertainty is indicated. This error bar does not include errors arising from the uncertainty in the inclination.

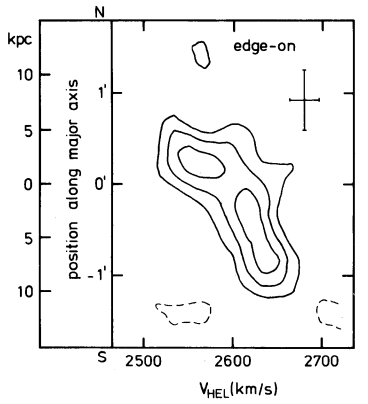

FIGURE 35. — Position-velocity plot along the major axis of the edge-on system (assumed position angle 170°). The resolution in velocity and in space is indicated by the cross. Contours are − 5.3, 5.3, 10.6 and 15.9 K brightness temperature. The negative contour is dashed ; the lowest positive contour lies on a 2 σ noise level.

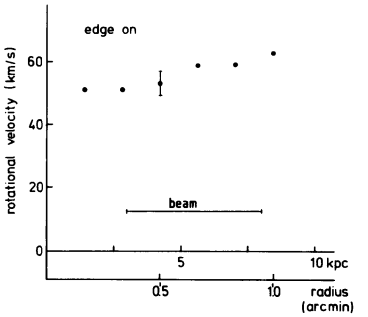

FIGURE 36. — Rotation curve of the edge-on system, as determined from fig. 35. No inclination correction has been applied since the inclination angle is likely to be very close to 90°.

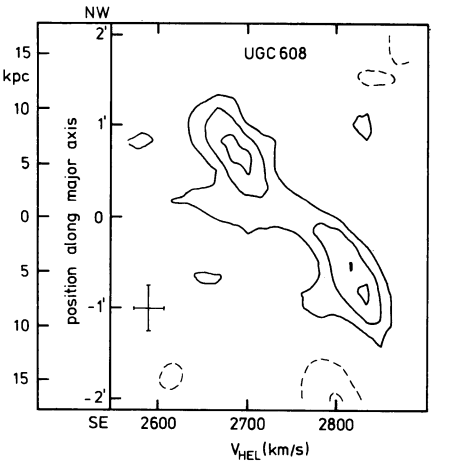

FIGURE 37. — Position-velocity plot along the major axis of UGC 608 (position angle 125°). Contours are − 8.4 (dashed), 8.4 (2 σ), 16.8 and 25.2 K brightness temperature.

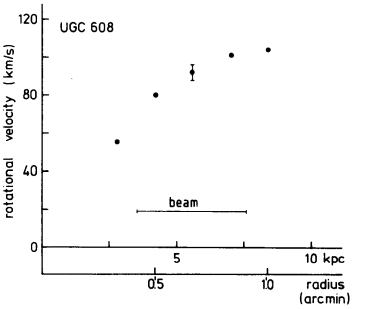

FIGURE 38. — Rotation curve of UGC 608, as determined from fig. 37. Rotational velocities have been corrected for an inclination of 66°.

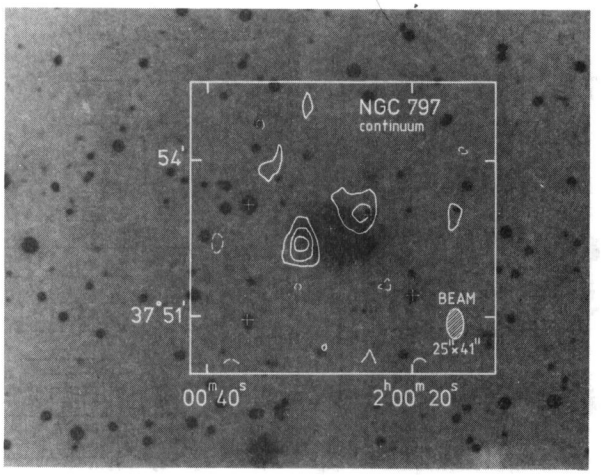

FIGURE 39. — Continuum map of NGC 797. The cross between the two sources marks the optical centre. The map has been corrected for primary beam attenuation. Contours are − 1.3 (dashed), 1.3 (2 σ noise level), 2.5 and 3.8 mJy/beam area.

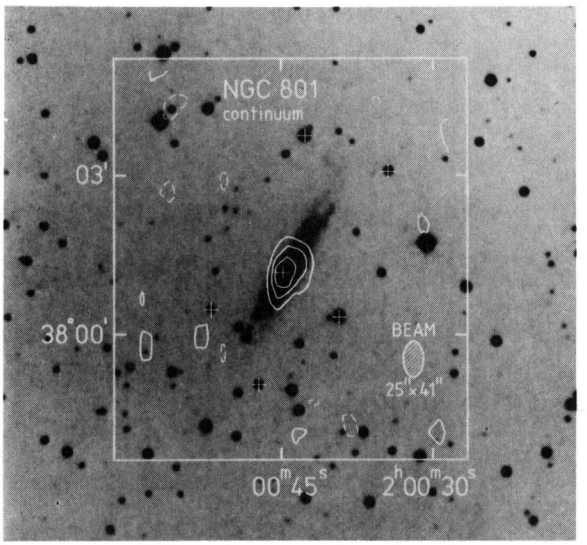

FIGURE 40. — Continuum map of NGC 801, corrected for primary beam attenuation. The optical centre is shown by the cross, coinciding with the centroid of the continuum emission. Contours are − 2.0 (dashed), 2.0, 4.0 and 6.0 mJy/beam area. The lowest contour corresponds to a 2 σ noise level. The noise level is different from that in fig. 39 since : a) different primary beam correction factors apply, and b) a different number of channels have been combined in creating the continuum maps.

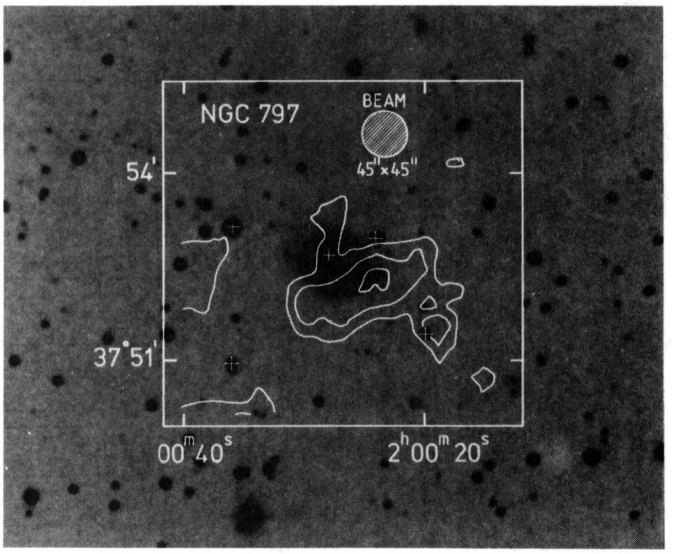

FIGURE 42. — HI distribution of NGC 797, corrected for primary beam effects. Contours are 1.2 (2 σ noise level), 2.3, and 3.5 × 10^{20} atoms/cm^2.

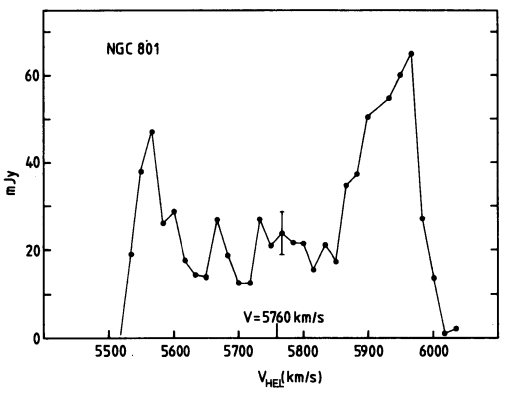

FIGURE 41. — Global HI profile for NGC 801, with a typical error bar and a preliminary systemic velocity indicated. For comparison, the systemic velocity of NGC 797 (not indicated) is 5 666 km/s.

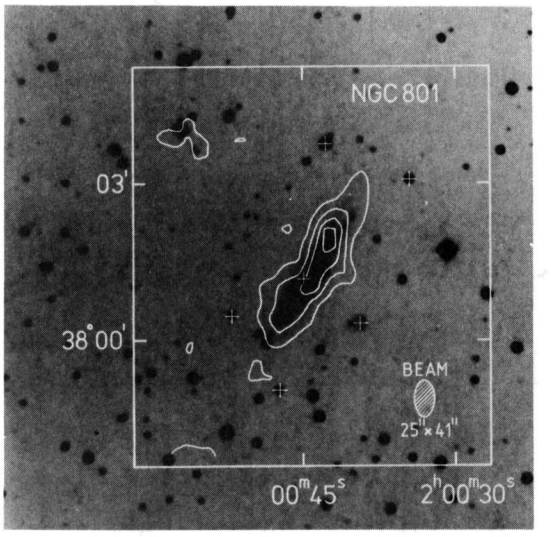

FIGURE 43. — HI distribution of NGC 801, corrected for primary beam effects. Contours are 4.3 (2.5 σ noise level), 12.9, 21.4 and 30.0 × 10^{20} atoms/cm^2.

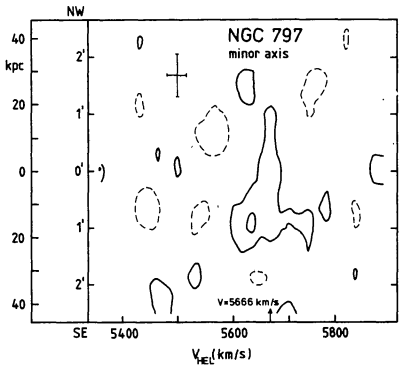

FIGURE 44. — Position-velocity plot of NGC 797 along the minor axis (position angle is 155°). The adopted systemic velocity is indicated on the velocity axis. Contours are − 3.5 (dashed), 3.5 (2 σ noise level), and 7.0 mJy/beam area.

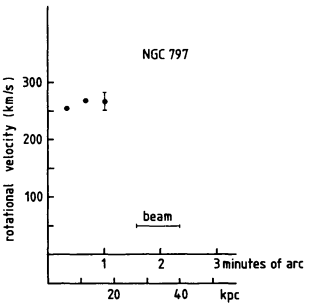

FIGURE 47. — Rotation curve of NGC 797, determined from fig. 45 using the systemic velocity from fig. 44. The indicated error bar does not include effects of an uncertain systemic velocity and inclination angle. The rotational velocities have been corrected for an inclination of 44°.

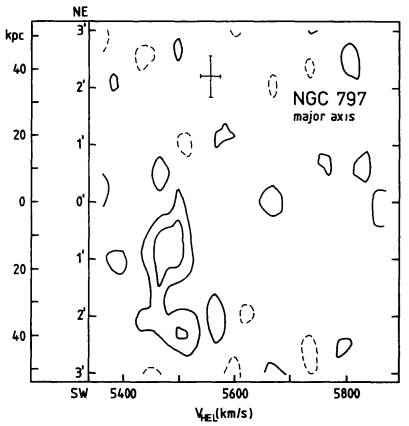

FIGURE 45. — Position-velocity plot of NGC 797 through the optical centre and with a position angle of 56° (cf. position angle major axis 65°). Contours are − 3.5 (dashed), 3.5 (2 σ noise level), and 7.0 mJy/beam area.

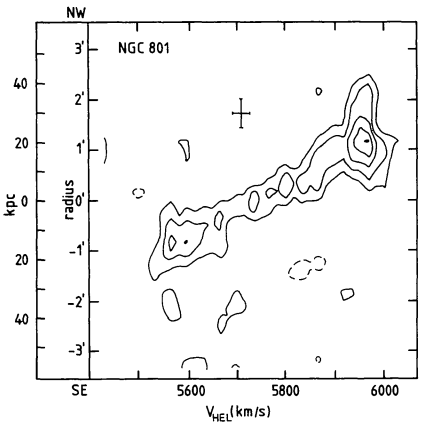

FIGURE 48. — Position-velocity plot of NGC 801 along its major axis (position angle 149°). The cross shows the resolution in velocity and in space. Contours are − 4.3 (dashed), 4.3 (2 σ noise level), 8.6, 12.9, 17.2 and 21.5 mJy/beam area.

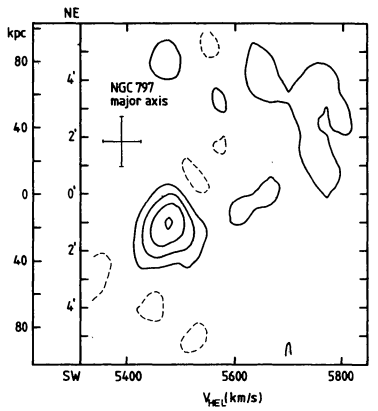

FIGURE 46. — Position-velocity plot of NGC 797 along the major axis, using data smoothed in space to a 100″ × 100″ beam, and in velocity to 67 km/s resolution. Resolutions are indicated by the cross. Contours are − 3.0, 0.3, 0.6, 0.9, and 1.2 K brightness temperature. The lowest contour corresponds to a 1.5 σ level.

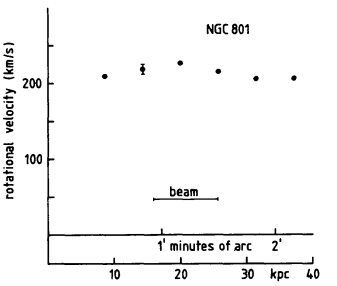

FIGURE 49. — Rotation curve of NGC 801, determined using fig. 48 and corrected for inclination. A typical uncertainty is indicated by the error bar.

ASTRONOMY & ASTROPHYSICS
SUPPLEMENT SERIES

OCTOBER 1983, PAGE 19

Astron. Astrophys. Suppl. Ser. **54**, 19-37 (1983)

Neutral hydrogen observations of double spiral galaxies. IV. NGC 4618/4625, NGC 4016/4017, NGC 3725/UGC 6528, UGC 725/728, NGC 2336/IC 467

G. A. van Moorsel

Kapteyn Astronomical Institute, University of Groningen, Postbus 800, 9700 AV Groningen, The Netherlands

Received April 15, accepted May 18, 1983

Summary. — Results of a 21 cm HI line study of five binary galaxies observed in the 21 cm HI line with the WSRT are presented. All ten galaxies were detected in HI, and systemic velocities and rotation curves were determined. The results are discussed in terms of a point mass model for the orbital motion in the pair. Only in the case of the pair NGC 4016/4017 a minimum orbital mass was found which did not exceed the sum of the individual masses. For the other four pairs the individual masses are not sufficient to account for the observed radial velocity differences. This suggests the presence of dark matter in the orbiting systems outside the radii of the individual galaxies.
In two galaxies, NGC 4625 and NGC 4017, the HI diameter exceeds the optical one by at least a factor 3. In the case of NGC 4017 the HI distribution is very suggestive of interaction with the companion.

Key words : HI observations — binary galaxies — redshifts.

1. Introduction.

This paper concludes the presentation of observations of a number of binary galaxy systems with the Westerbork Synthesis Radio Telescope (WSRT) in the 21 cm line of neutral hydrogen. In previous publications (Van Moorsel, 1982 (paper I), 1983a (paper II) and 1983b (paper III)) the observations of nine binary systems are given ; the remaining five are described here.

Details about the motivation for observing binary galaxies using the WSRT and the criteria used to select the sample are discussed in paper I.

The WSRT can observe virtually every pair in one 12 hours synthesis observation, and has at the same time sufficient resolution to provide detailed maps of the individual galaxies. The latter circumstance allows the determination of a rotation curve. The difference in radial velocity sets a minimum to the total mass of the binary system. This value is compared with the sum of the two individual masses, determined by means of the rotation curves. This comparison can ultimately lead to conclusions concerning the distribution of mass in binary systems.

The five pairs to be discussed in this paper are :

i NGC 4618/4625
ii NGC 4016/4017
iii NGC 3725/UGC 6528
iv UGC 725/728
v NGC 2336/IC 467.

Section 2 contains a brief general description of these five binary systems, in section 3 techniques concerning observations and reduction are summarized, section 4 contains the presentation of the results of the observations, and in section 5 the results are summarized and briefly discussed.

2. Description of the pairs.

NGC 4618/NGC 4625.

An optical photograph which involves this pair is shown in figure 1. The angular separation is 8 arcmin, which corresponds to 15 kpc at an adopted distance of 6.3 Mpc (H = 100 km/s/Mpc throughout this paper). Both galaxies are classified as Sc (Nilson, 1973), but spiral arms are hard to trace. Their appearance is disturbed, suggesting mutual interaction. The derived inclinations for NGC 4618 and NGC 4625 (35° and 27° respectively) are based on the axial ratios given in the Uppsala Catalogue (Nilson, 1973) and the Second Reference Catalogue (de Vaucouleurs, 1976).

NGC 4016/NGC 4017.

This pair, shown in figure 2, consists of two optically small (diameter < 2′) galaxies. NGC 4016 is a faint ($14^m.6$) galaxy of type SBc-Irr (Nilson, 1973) and NGC 4017 a more luminous ($13^m.5$) spiral of type Sb-SBc (Nilson, 1973). From the observed redshifts a distance of 34.3 Mpc is derived. The angular separation of the pair members is 6.4 arcmin (64 kpc).

NGC 3725/UGC 6528.

These very similar looking galaxies are shown in figure 3. NGC 3725, the brighter of the two ($13^m.6$), is situated 8 arcmin east of UGC 6528 ($14^m.1$). Both galaxies show clear indications of spiral structure, but the individual arms are hard to trace. NGC 3725 is of type SBc, though the bar is not visible in the reproduction, and UGC 6528 is of type Sc. Magnitudes and types are given in the UGC (Nilson, 1973). This pair has been observed previously by Peterson (1979) in his HI binary galaxy survey. The adopted distance is 34.1 Mpc, implying a projected physical separation of 75 kpc.

UGC 725/UGC 728.

This double system, consisting of two late type — possibly barred — spirals is shown in figure 4. The systemic velocities indicate a distance of 52 Mpc. The angular separation is 11.3 arcmin (170 kpc). A source of uncertainty in the interpretation of the results for UGC 728 is formed by the uncertain inclination. Determinations of inclinations based on optical extents are bound to be unrealistic when the extent is mainly determined by the spiral arms, as in the case of UGC 728. In this paper an inclination of 45° is adopted.

NGC 2336/IC 467

Figure 5 shows the pair NGC 2336/IC 467. NGC 2336 is a bright (m_{pg} = 11.3) late type spiral with well developed spiral arms along which a number of prominent HII regions is visible. Its type is SBc (Nilson, 1973). The HI in this galaxy has been observed in a number of single dish surveys (Shostak, 1978 ; Dickel and Rood, 1978 ; Rots, 1980). The inclination used in this paper is 59° (Nilson, 1973 ; de Vaucouleurs *et al.*, 1976). IC 467 (m_{pg} = 12.7) is also a late type spiral, with less prominent arms than those of NGC 2336. It is of type Sc and is seen at an inclination of 69°.

A distance of 22.9 Mpc was adopted for this pair. The angular separation of 20.2 arcminutes then corresponds to a projected linear separation of 135 kpc.

3. Observations and reduction

The five fields were mapped with the Westerbork Synthesis Radio Telescope and the digital line backend. Parameters of the observations are listed in table I. The observation of the last pair, NGC 2336/IC 467, benefited considerably from the presence of new cooled frontends on the movable telescopes, resulting in a reduction in noise by a factor 2 compared with older observations.

The data reduction involves the following steps : after calibration the data are Fourier transformed, resulting in 63 channel maps evenly spaced in frequency with a velocity coverage of $\simeq$ 1 000 km/s. A continuum map, formed by averaging channel maps free of line emission, is subtracted from all the line channels. All resulting maps undergo a cleaning procedure to remove the instrumental effects inherent to the chosen telescope configuration (minimum spacing 72 meters, see Table I). This cleaning also removes the instrumental grating rings which are caused by the 72 m spacing increment. In a few cases these rings interfere with the emission from the companion galaxy. Systemic velocities and rotation curves are derived either from the velocity field, in cases where the inclination is low ($< 60°$) and resolution effects are not significant (Warner *et al.*, 1973), or from the position-velocity plot along the major axis in the remaining cases (Sancisi and Allen, 1979). The former method essentially fits a model velocity field to the observed field by varying various parameters, the latter method attempts to correct for beam smearing by adopting at every point on the major axis the velocity of the corresponding profile which differs most from the systemic velocity. A more detailed description of these methods is given in paper I. Systemic velocities allow the determination of the minimum orbital mass M_{orb} (Paper I, and references therein), and the rotation curves give the total individual masses (Nordsieck, 1973). The HI mass was calculated from the integrated emission, assuming no internal absorption. The values given represent therefore only lower limits to the true values.

4. Results.

NGC 4618/NGC 4625

As shown in figure 6, NGC 4618 shows bright extended continuum emission over its optically visible disk ; in NGC 4625, however, the continuum emission is close to the the detection limit. Figure 8 shows the large HI sizes of both galaxies with respect to the optical dimensions. Note, however, that NGC 4625 also shows very faint optical emission beyond the boundary of the bright optical disk, but this faint emission was not used by Nilson in the determination of the optical diameter. The wide HI extent became visible only after convolution of the channel maps to a $45'' \times 45''$ beam. Note that — in spite of the apparent proximity of the two galaxies — no clear signs of tidal distortion are present in the distribution of HI.

Figure 10 shows a severely distorted velocity field for NGC 4618, and a much more regular one for NGC 4625. The rotation curve of NGC 4618 in figure 11 was determined assuming the dashed line in figure 10 follows the kinematical major axis. A second indication of the presence of tidal effects are the unusually large widths of the velocity profiles in NGC 4618, indicating larger random velocities ($\simeq$ 20 km/s) than observed in non-perturbed galaxies ($\simeq$ 10 km/s, Van der Kruit, 1981). The last 6 points on the rotation curve of NGC 4618 in figure 11 are possibly overestimated since there are indications that the inclination increases with radius. This causes an extra uncertainty in the derived total mass. In contrast, the kinematics of NGC 4625 are hardly affected.

NGC 4016/NGC 4017.

The continuum map in figure 13 shows that both galaxies emit detectable continuum radiation. The centroid of the emission from NGC 4016 coincides with

the optical position measured by the author on a PSS print, and is 1.6 arcminutes off with respect to the value given by Nilson (1973). The continuum emission from NGC 4017 is extended in the east-west direction.

The HI results are all based on maps convolved to a 45″ × 60″ beam. In the total HI map in figure 15 the enormous extent of HI associated with NGC 4017 is obvious. The outer parts are strongly reminiscent of the damage incurred in a close encounter. The third small HI concentration in the north probably is a continuation of the tail of NGC 4017.

The large beam and the small angular size of NGC 4016 cause the details in the derived rotation curve (Fig. 18) to be very uncertain. The velocity field of NGC 4017 shows that the kinematical major axis position angle agrees with the direction in which the HI extent is maximal. This suggests that most of the extended HI outside the optical galaxy is distributed fairly symmetrically in the plane of this galaxy. From the shape of the HI distribution the inclination appears to be higher than the one given by Nilson (1973) from the optical dimensions alone. The latter value is certainly strongly influenced by the extent and shape of the optical spiral arms. In the present paper a 45° inclination is used rather than Nilson's 34°, but the inclination might well be as large as 60°. In determining the rotation curve of NGC 4017 the northward pointing tail was not included in the analysis, in view of the uncertain orientation with respect to the plane of the galaxy.

NGC 3725/UGC 6528.

The detection of HI in NGC 3725 was marginal, and the global profile proved to be too noisy and too dependent of the area of integration to be of any significant use. The global profile of UGC 6528 in figure 23 is identical to the instrumental profile convolved with a 10 km/s wide gaussian representing the random motions in the galaxy. This indicates that this galaxy is oriented almost face-on. Convolution to a 40″ × 40″ beam improved the significance of the detection of HI associated with NGC 3725 (Fig. 24) ; for UGC 6528, however, original maps were used (Fig. 25).

The marginal HI detection in NGC 3725 increases the uncertainties in the kinematical results in this galaxy. For UGC 6528 no rotation information is available apart from an upper limit. Its mass was estimated assuming a mass-to-luminosity ratio equal to that of NGC 3725. The similar optical appearence suggests that this assumption is valid.

UGC 725/UGC 728.

Figures 29 and 30 show that these two galaxies have regular and apparently undisturbed HI distributions. Also their kinematics are characterized by the lack of any significant deviation from symmetry. In the case of UGC 728, as for NGC 4017, the uncertainty stems mostly from the fact that the inclination of the orbital plane is not known accurately. The position angle of major axis, however, could be determined with enough accuracy using the centroids of the HI distributions in the individual channel maps.

NGC 2336/IC 467.

The integrated HI emission from NGC 2336 as determined from figure 35, namely 60.9 Jy.km/s, can be compared with previously obtained values :

i) 42,5 Jy.km/s (Dickel and Rood, 1978). This result is based on a very noisy global profile, which might well introduce differences as large as the one observed.

ii) 59.8 Jy.km/s (Rots, 1980). This value agrees well with the presently found one. Rots' suggestion that his value might be underestimated due to possible poor baseline fitting caused by the low surface brightness of NGC 2336 does not seem to be confirmed by the present data.

iii) 81.3 Jy.km/s (Shostak, 1978). This value tends to support Rots' suggestion. It is not obvious, however, that in this case the baseline fitting is more reliable than under ii). Moreover, it is very unlikely that a substantial fraction of low brightness extended HI was missed in the present observation.

The low HI surface brightness in NGC 2336 required a convolution of the channel maps to a 35″ × 35″ beam. The most striking feature of the HI map in figure 36 is the HI hole at the location of the optical centre. There are no signs of major disturbances. For IC 467 unsmoothed 25″ × 25″ data were used.

Both galaxies show very regular kinematics. The apparent deviations from a symmetrical velocity field which are visible due north of the centre of NGC 2336 in figure 39 originate from the steep gradient in HI column density at these locations, and have nothing to do with the presence of non-circular motions, as would seem to be the case at the first glance.

5. Discussion.

Table II summarizes the results of the five pairs, described in the previous section. For each galaxy and each pair only those parameters are given which are directly relevant for the mass determination. These include the mass per galaxy m_i, determined from the corresponding rotation curve, and the minimum orbital mass, M_{orb}, calculated from the radial velocity difference Δv. The dimensionless ratio $\chi_{obs} \equiv M_{orb}/\Sigma m_i$ is given in column 7. In a future paper the distribution of this ratio in the total sample will be further analysed.

NGC 4618/NGC 4625.

This pair has a χ_{obs} value 2.2, well above the theoretical maximum 1.0 (Van Moorsel, paper I). The error in χ_{obs}, however, is large, which implies that values below 1.0 for the pair are possible, if unlikely. The high error in χ_{obs} is caused by the uncertain individual masses of NGC 4618 and NGC 4625, which are a result of the low inclinations of the two galaxies.

NGC 4016/NGC 4017.

The χ_{obs} of this pair is close to zero, in agreement with the picture in which the two galaxies are separate mass concentrations in orbital motion around their centre of gravity. The mass difference between NGC 4016 and NGC 4017 is so large that the former may be considered as a satellite of the latter.

NGC 3725/UGC 6528.

Since no kinematical information on UGC 6528 is present in our data, the usual procedure of calculating a total mass from the rotation curve cannot be followed. Instead, the same M/L ratio is assumed for NGC 3725 and UGC 6528. This assumption appears justified by the similar optical appearence of the two galaxies. Although the resulting χ_{obs} value is rather uncertain, there can be little doubt that it is greater than 1.

UGC 725/UGC 728.

This pair definitely has a χ_{obs} well above 1. The uncertainty in χ_{obs} is primarily due to the imprecise mass of UGC 728, a consequence of the poorly determined inclination of this galaxy.

NGC 2336/IC 467.

Both the individual masses and the orbital mass can be accurately determined for this pair, resulting in an uncertainty in χ_{obs} of less than 25 %. Again χ_{obs} lies significantly above 1.

In summary, it is striking that the observed values of χ_{obs} tend to be higher than the theoretical maximum of 1.0, assuming a two body model and circular orbits, and much higher than the theoretical average value, which ranges between 0.2 and 0.4, depending on the influence of selection criteria and the character of the orbits. This implies that a two body model, with masses given by the rotation curves, is inappropriate for at least a substantial fraction of the binary systems. The presence of dark matter in these systems is thereby indicated. These questions are addressed in detail in a future paper.

Acknowledgments.

This work would have been impossible without the help of the following people : the staff of the Netherlands Foundation for Radio Astronomy, the programming group at the Kapteyn Astronomical Institute, W. Haaima and his associates who took care of the photography, and the secretarial staff at this Institute.

A special word of thanks goes to T.S. van Albada, R. Sancisi, and G.S. Shostak for their advice, critical reading of, and valuable comments on the manuscript, and to Z.W.O. for financial support.

The Westerbork Synthesis Radio Telescope is operated by the Netherlands Foundation for Radio Astronomy which is financially supported by the Netherlands Organization for the Advancement of Pure Research (Z.W.O.).

References

DICKEL, J. R. and ROOD, H. J. : 1978, *Astrophys. J.* **223,** 391.
DRESSEL, L. L. and CONDON, J. J. : 1976, *Astrophys. J. Suppl. Ser.* **31,** 187.
KRUIT, P. C. VAN DER : 1981, *Astron. Astrophys.* **99,** 298.
MOORSEL, G. A. VAN : 1982, *Astron. Astrophys.* **107,** 66 (paper I).
MOORSEL, G. A. VAN : 1983a, *Astron. Astrophys. Suppl. Ser.* **53,** 271 (paper II).
MOORSEL, G. A. VAN : 1983b, *Astron. Astrophys. Suppl. Ser.* (this volume) **54,** 1 (paper III).
NILSON, P. : 1973, *Uppsala General Catalogue of Galaxies,* Uppsala Astron. Obs. Ann. 6.
NORDSIECK, K. H. : 1973, *Astrophys. J.* **184,** 719.
PETERSON, S. : 1979, *Astrophys. J.* **232,** 20.
ROTS, A. H. : 1980, *Astron. Astrophys. Suppl. Ser.* **41,** 189.
SANCISI, R. and ALLEN, R.J. : 1979, *Astron. Astrophys.* **74,** 73.
SHOSTAK, G. S. : 1978, *Astron. Astrophys.* **68,** 321.
VAUCOULEURS, G. de, VAUCOULEURS, A. de, CORWIN, H. G. : 1976, *Second Reference Catalogue of Bright Galaxies,* University of Texas Press, Austin.
WARNER, P. J., WRIGHT, M. C. H., BALDWIN, J. E. : 1973, *Mon. Not. R. Astron. Soc.* **163,** 163.
ZWICKY, F., HERZOG, E., KARPOWICZ, M., KOWAL, C. T., WILD, P. : 1961-1968, *Catalogue of Galaxies and of Clusters of Galaxies,* Vols. 1-6, Pasadena, California Institute of Technology.

TABLE I. — *Parameters of the observations.*

Name	NGC 4618/NGC 4625	NGC 4016/NGC 4017	NGC 3725/UGC 6528	UGC 725/UGC 728	NGC 2336/IC 467
date of observation	3 September 1979	8 September 1979	9 September 1979	25 November 1979	24 January 1981
length of observation (hours)	12	12	12	12	12
number interferometers	18	18	18	18	20
baselines (m) (min-max-increment)	72-1296-72	72-1296-72	72-1296-72	72-1296-72	72-1440-72
synthesized beam (sec. of arc)	27 × 41	27 × 59	27 × 31	28 × 42	24 × 25
radii first grating ring (min. of arc)	10.2 × 15.4	10.2 × 21.8	10.2 × 11.5	10.2 × 15.0	10.2 × 10.4
FWHP primary beam (min. of arc)	37.6	37.6	37.6	37.6	37.6
rms noise channel maps (K)	1.0	0.7	1.4	0.9	0.8
velocity central channel (km/s) (heliocentric)	450	3300	3200	4980	2100
bandwidth (MHz)	5	5	5	5	5
number of frequency channels	63	63	63	63	63
channel separation (km/s)	16.5	16.9	16.8	17.0	16.7
velocity resolution (km/s)	33	34	34	34	33
R.A. field centre (1950) (h, m, s)	12 39 12	11 55 54	11 30 18	01 07 28	07 20 00
Dec. field centre (1950) (°, ', ")	41 31 00	27 45 00	62 09 00	42 55 00	80 05 00
mJy-K conversion, equivalent of 1.0 K (mJy/beam area)	1.8	2.6	1.3	1.9	1.0
same for smoothed maps	4.0	4.3	2.6	-	2.0

TABLE II. — *Data and results.*

1-	4618	4625	4016	4017	3725	-	-	-	2336	I467
2-	7853	7861	6954	6967	6542	6528	725	728	3809	3834
3-	Sc	Sc	SBc-Irr	Sb-SBc	SBc	Sc	SB(?)c	Sc-SBc	SBc	Sc
4-	11.5	13.0	14.6	13.5	13.6	14.1	14.5	14.2	11.3	12.7
5-	12 39 09.5	12 39 29.6	11 55 54.9§	11 56 11.1	11 30 52.4	11 29 55.0	01 07 17.9	01 07 36.5	07 18 28.0	07 21 56.3
6-	41 25 29	41 32 53	27 48 30§	27 43 57	62 09 50	62 06 14	42 50 34	43 01 19	80 16 35	79 58 30
7-	-	8.3	-	5.8	-	7.6	-	11.3	-	20.2
8-	35	27	60	45	41	< 4	79	45	59	68
9-	4.5	1.5	1.5	1.8	1.6	1.2	2.2	1.5	7.0	3.5
10-	5.7	2.4	2.0	2.6	2.4	2.0	2.3	2.2	7.3	3.8
11-	6.3(8.3)*	6.3(7.8)*	2.6	7.3	2.4	1.7	3.4	2.9	8.2	4.8
12-	537 ± 6	611 ± 5	3432 ± 6	3452 ± 6	3336 ± 8	3251 ± 8	5041 ± 5	4907 ± 6	2199 ± 4	2040 ± 5
13-	6.3		34.3		34.1		52.0		22.9	
14-	47.2	29.7	7.5	25.8	3.0	1.6	9.3	11.2	60.9	20.2
15-	4.4	2.8	21	71	8	4	59	71	75.2	24.9
16-	78	64	81	216	113	-	159	189	256	157
17-	0.5	0.4	1.7	16.2	2.7	-	8.3	10.1	31	5.1
18-	38 ± 2	10 ± 2	8 ± 1	22 ± 2	9 ± 2	< 1.8	< 2.5	< 2.5	< 1.2	< 1.0
19-	variable	132	177	126	153	-	43	103	179	70

Notes to table II

1 NGC number or — if preceded by I — IC number.
2 UGC number.
3 Morphological type (from the UGC, Nilson, 1973).
4 Apparent photographical magnitude (from the CGCG, Zwicky *et al.*, 1961-1968).
5 Right Ascension of galaxy centre (1950.00) in h, m, s. From Dressel and Condon (1976), or using a central continuum source.
6 Declination of galaxy centre (1950.00) in °, ′, ″. From Dressel and Condon (1976), or using a central continuum source.
7 Distance to first galaxy in the pair (arcmin).
8 Inclination angle of plane of galaxy (°). From the UGC (Nilson, 1973), and the Second Reference Catalogue (de Vaucouleurs *et al.*, 1976).
9 Blue diameter in arcmin (Nilson, 1973).
10 Holmberg diameter in arcmin. Due to lack of photometry on these galaxies the empirical relation

$$d_H = 1.75.a^{0.84}.(b/a)^{0.3}$$

is used (Dickel and Rood, 1978). Here a is the blue diameter (see 9), b the minor axis diameter, and d_H the empirically determined Holmberg diameter.
11 Largest extent of HI (arcmin), using the 2×10^{20} atoms/cm^2 contour. An asterisk indicates the HI diameter based on the 1.2×10^{20} atoms/cm^2 contour.
12 Systemic velocity (km/s) as determined in this paper.
13 Distance in Mpc using the mean radial velocity corrected by 300 sin l cos b (l and b are galactic coordinates), and a Hubble constant of 100 km/s/Mpc.
14 Total HI emission (Jy.km/s).
15 Total HI mass in units of 10^8 $M_\odot$.
16 Maximum rotation velocity (km/s).
17 Total mass in units of 10^{10} $M_\odot$.
18 Continuum flux (mJy). An upper limit gives the 3 σ noise level in mJy/beam area.
19 Position angle of the major axis, measured from north eastward.

TABLE III. — *Summary of results.*

1 NGC	2 UGC	3 radius (kpc)	4 m (10^{10} $M_\odot$)	5 Δv (km/s)	6 M_{orb} (10^{10} $M_\odot$)	7 $M_{orb}/\Sigma m_i$
4618	7853	7	0.9 ± 0.3	74 ± 7	1.9 ± 0.4	2.2 ± 1.3
4625	7861	6				
4016	6954	15	17.7 ± 4.0	20 ± 8	0.6 ± 0.4	< 0.06
4017	6967	35				
3725	6542	13	4.4 ± 1.5	85 ± 11	13 ± 3	3.0 ± 1.8
-	6528	-				
-	725	22	18.3 ± 4.0	134 ± 8	71 ± 9	3.9 ± 1.5
-	728	18				
2336	3809	31	36 ± 5	159 ± 7	79 ± 6	2.2 ± 0.5
IC467	3834	13				

Notes to table III

Column	Note
3	Distance from centre to outermost point on the rotation curve.
4	Sum of rotation curve masses. The error includes uncertainties in the inclination angle, but not effects of a different mass distribution (e.g. spherical rather than a flat disk).
5	Difference in radial velocities as given in table II.
6	Minimum orbital mass, calculated as $M_{orb} = 6.7 \times 10^4 (\Delta v)^2.\Delta R.D$, with Δv, ΔR, and D given in column 5 and table II.
7	Ratio of minimum orbital mass in column 6 and the sum of the individual masses in column 4 (χ_{obs}).

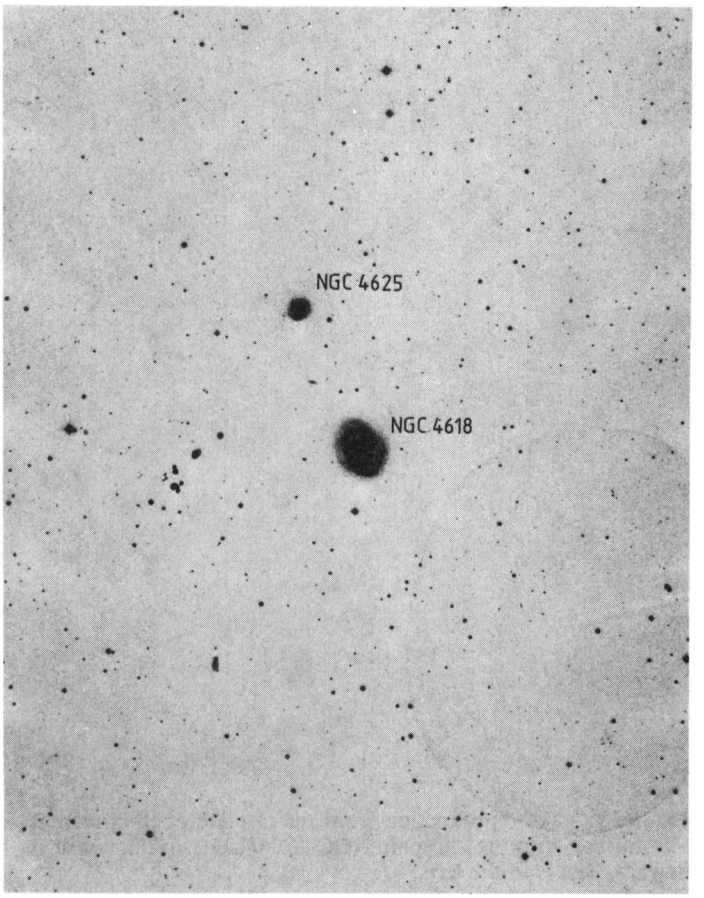

FIGURE 1. — A reproduction of the Palomar Sky Survey O print showing the region around the pair NGC 4618/4625. North is upward, east is to the left.

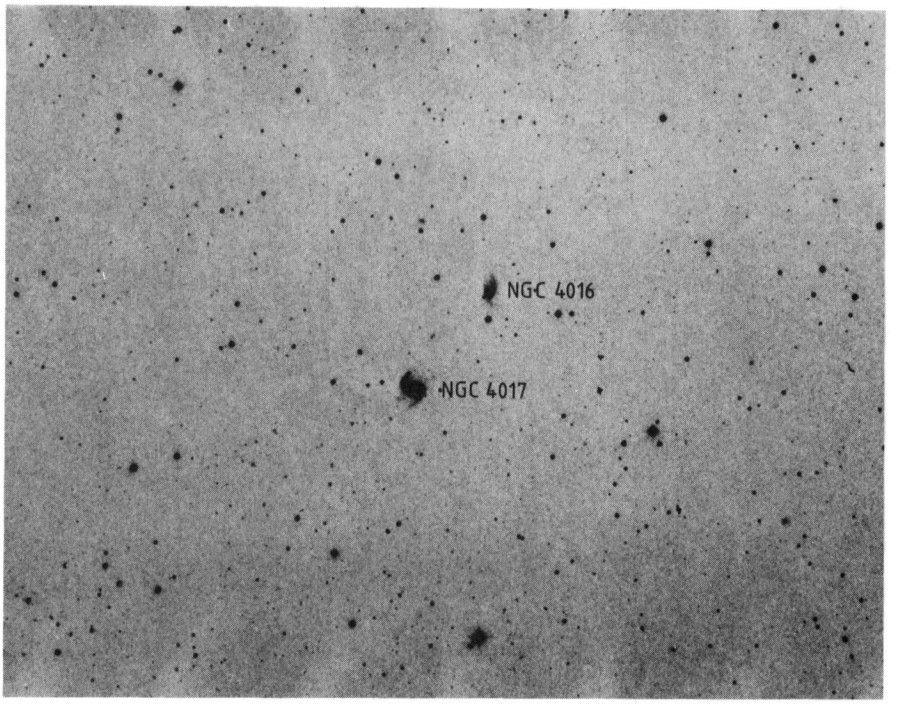

FIGURE 2. — The pair NGC 4016/4017 on a reproduction from a O print of the Palomar Sky Survey. North is upward, east is to the left.

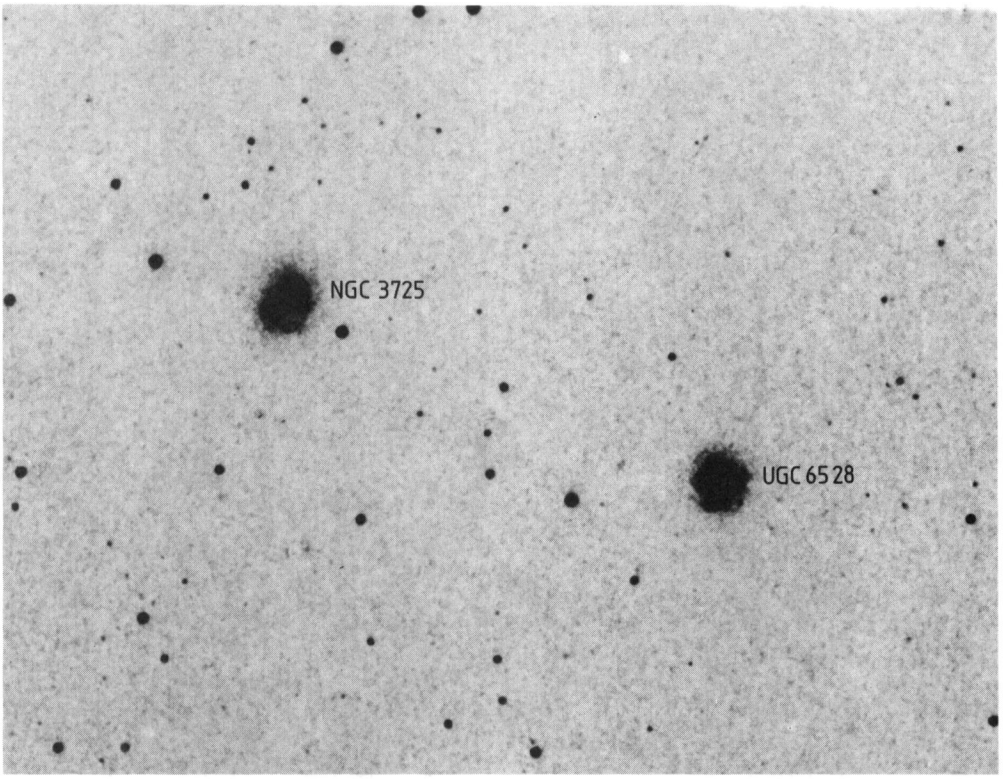

FIGURE 3. — A reproduction from the O plate of the Palomar Sky Survey showing the pair NGC 3725/UGC 6528. North is upward, east is to the left.

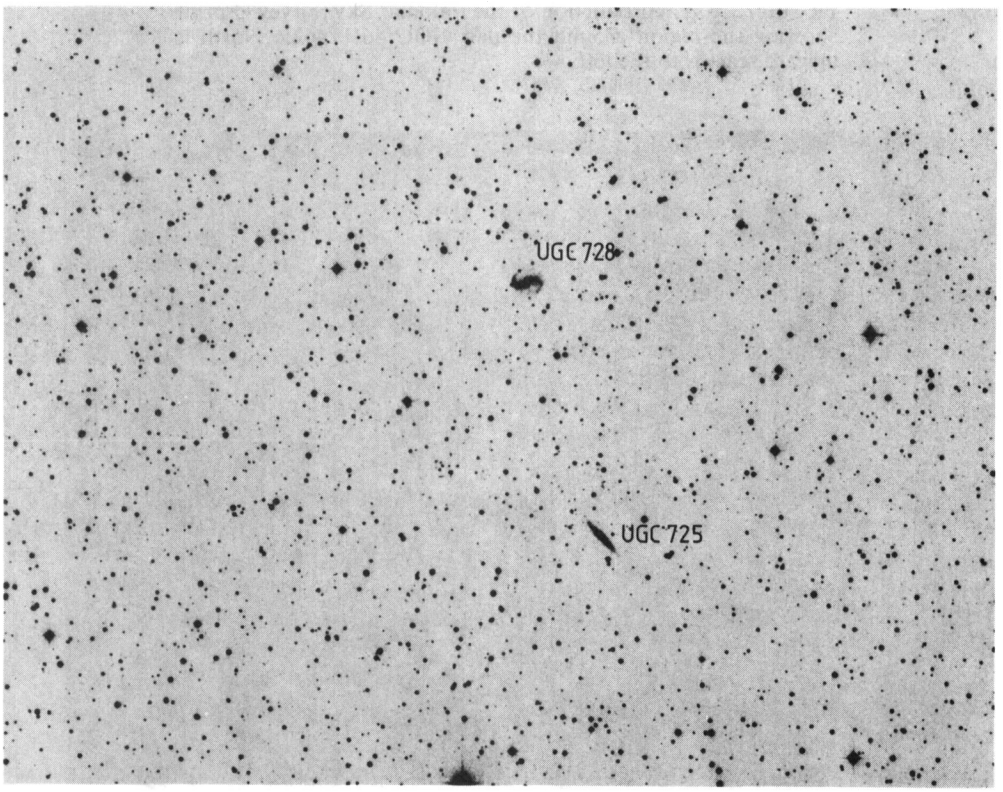

FIGURE 4. — The pair UGC 725/728 on a reproduction from an O plate of the Palomar Sky Survey. North is upward, east is to the left.

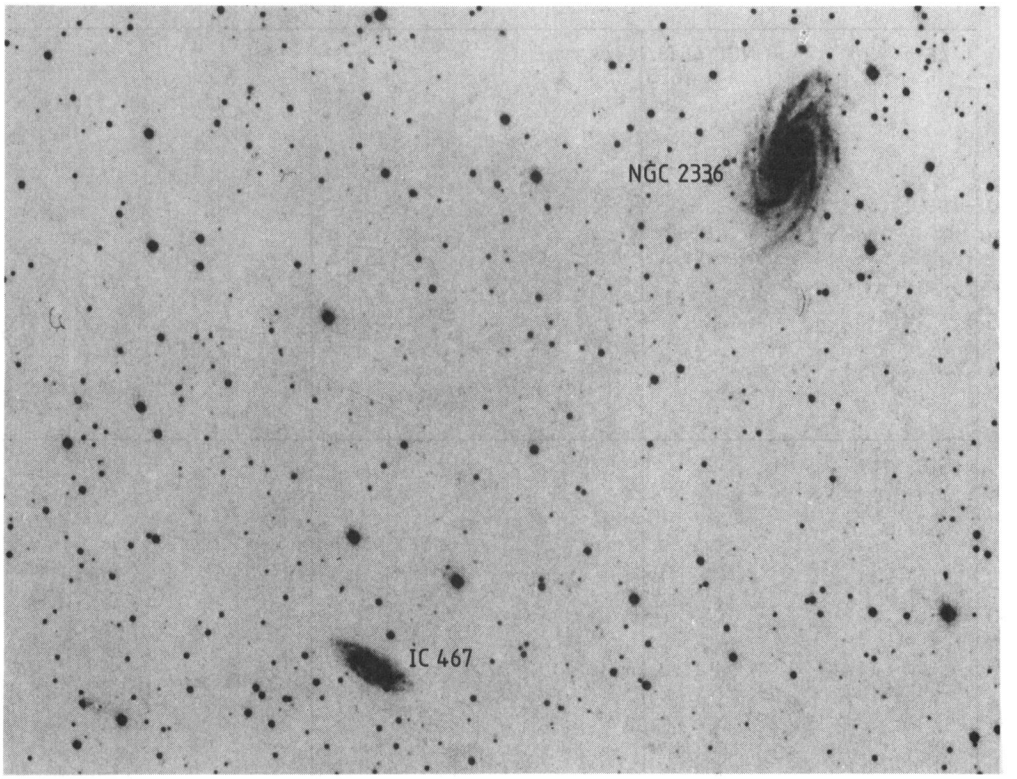

FIGURE 5. — The pair NGC 2336/IC 467 on the O plate of the Palomar Sky Survey. North is directed up, east is to the left.

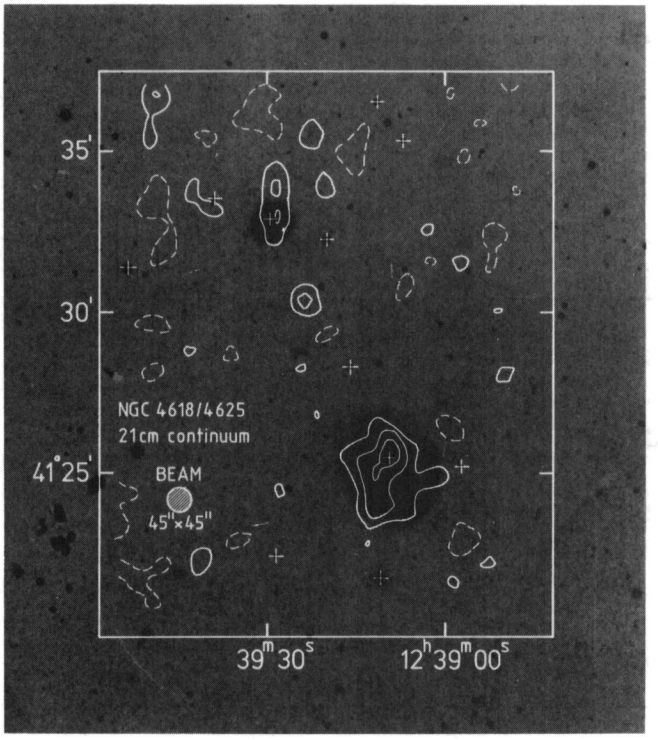

FIGURE 6. — Continuum map of the region around NGC 4618 and NGC 4625. Interfering instrumental grating rings of some background sources have been removed. Contours are − 1.5, 1.5 (2 σ), 3.0, and 4.5 mJy/beam area.

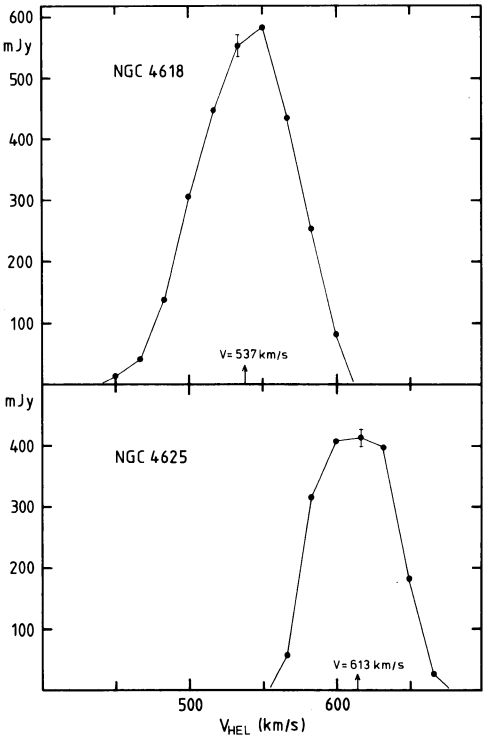

FIGURE 7. — Global HI profiles of NGC 4618 and NGC 4625. Flux densities are corrected for primary beam attenuation. Systemic velocities, derived from the profile edges, are included in the figure.

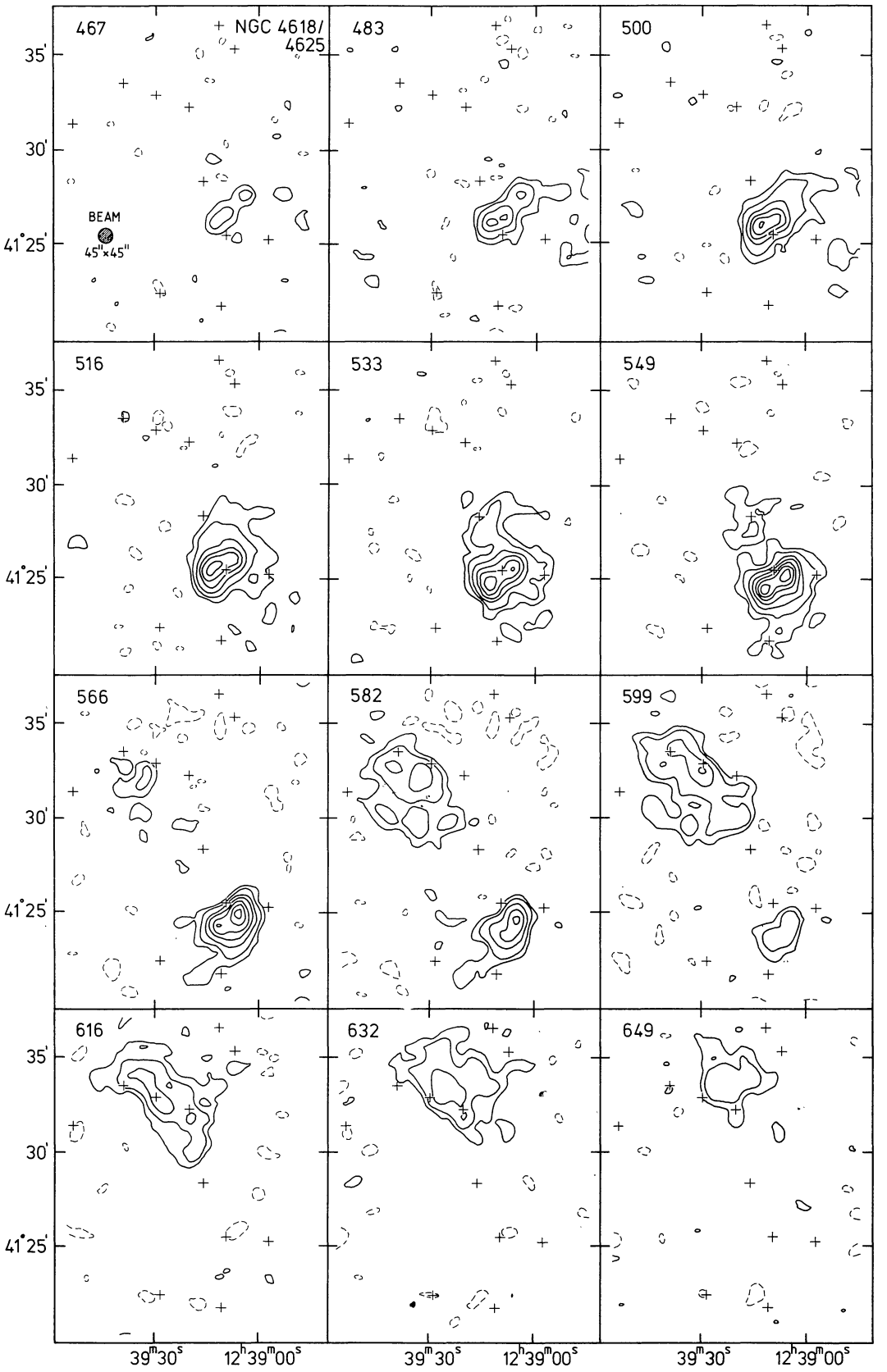

FIGURE 9. — Consecutive channel maps of the pair NGC 4618/NGC 4625. Numbers in the upper left corners refer to the corresponding heliocentric velocities. The crosses are the same as in figure 8. Contours are − 1.2, 1.2, 2.4, 7.1, 9.4, 11.8, and 14.1 K brightness temperature. The lowest contour (1.2 K) corresponds to a 2.5 σ noise level.

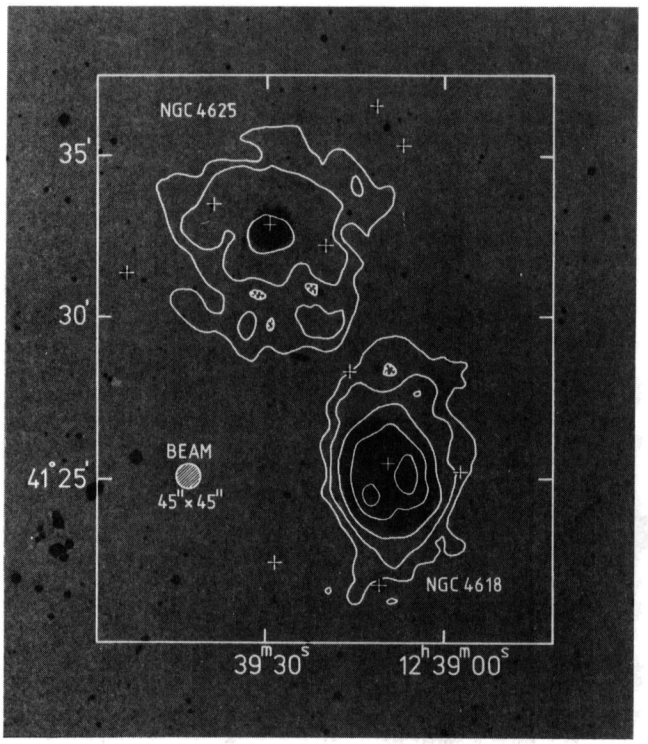

FIGURE 8. — Total HI map of NGC 4618 and NGC 4625. Contours are 1.2, 2.3, 4.6, 9.2, and 13.9 × 10^{20} atoms/cm^2. The lowest contour corresponds approximately to a 2.5 σ noise level. The central crosses mark the positions of the optical centres.

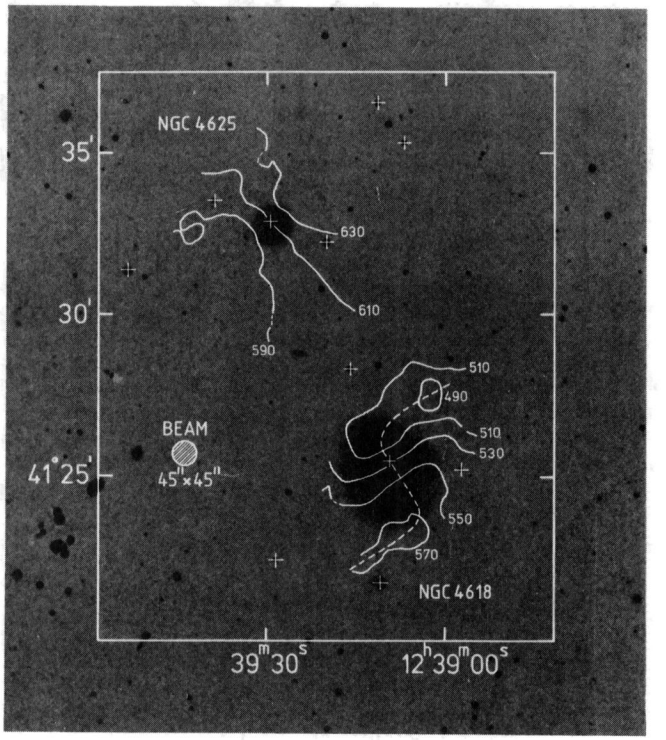

FIGURE 10. — Velocity field of the pair NGC 4618/NGC 4625. The contours are labelled with the heliocentric radial velocities. The major axis adopted for NGC 4618 is indicated by the dashed line.

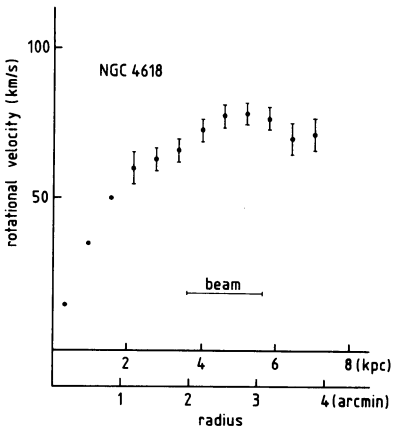

FIGURE 11. — Rotation curve of NGC 4618, assuming a major axis as drawn in figure 10. The inner points are affected by resolution effects ; therefore no error bars are given. Rotational velocities have been corrected for the adopted inclination of 35°. Uncertainties in the inclination have not been included in the error bars.

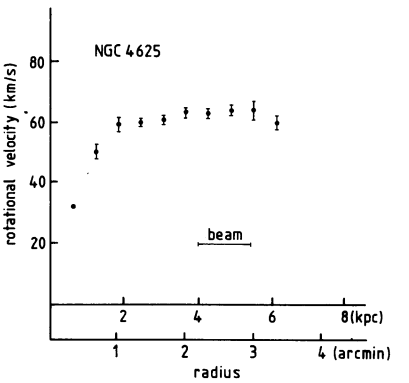

FIGURE 12. — Rotation curve of NGC 4625, determined from the velocity field in figure 10. Velocities have been corrected for an inclination angle of 27°. Uncertainties in the inclination have not been included in the error bars.

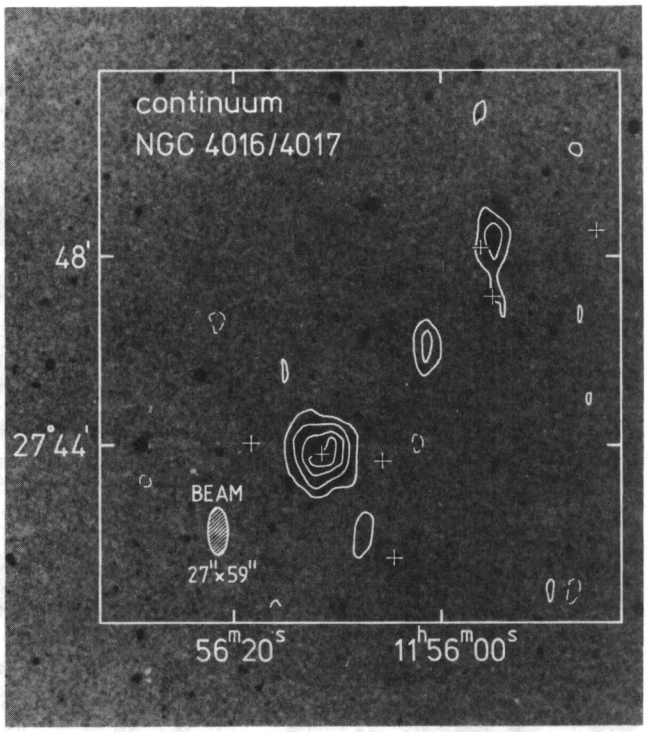

FIGURE 13. — Continuum map of the galaxies NGC 4016 and NGC 4017. Contours are − 1.5, 1.5, 3.0, 4.5 and 6.0 mJy/beam area. The lowest contour corresponds to 2.3 σ rms noise in the map.

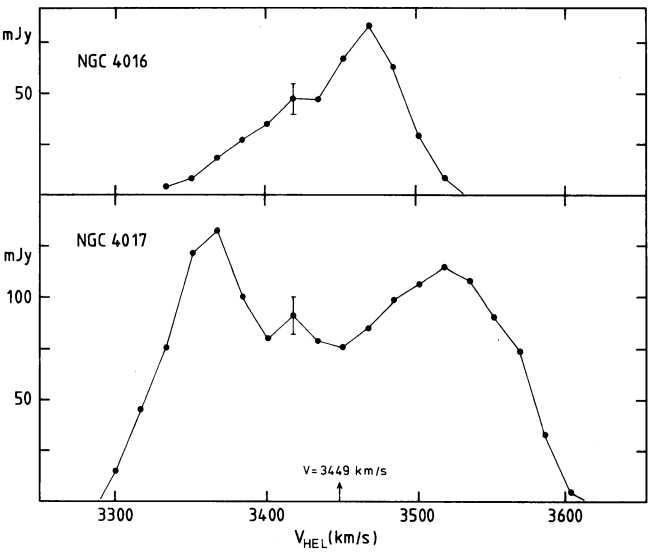

FIGURE 14. — Global profiles of NGC 4016 and NGC 4017, corrected for primary beam attenuation. The systemic velocity of NGC 4017, as derived from the profile, is indicated. The profile of NGC 4016 is too asymmetric to determine a systemic velocity.

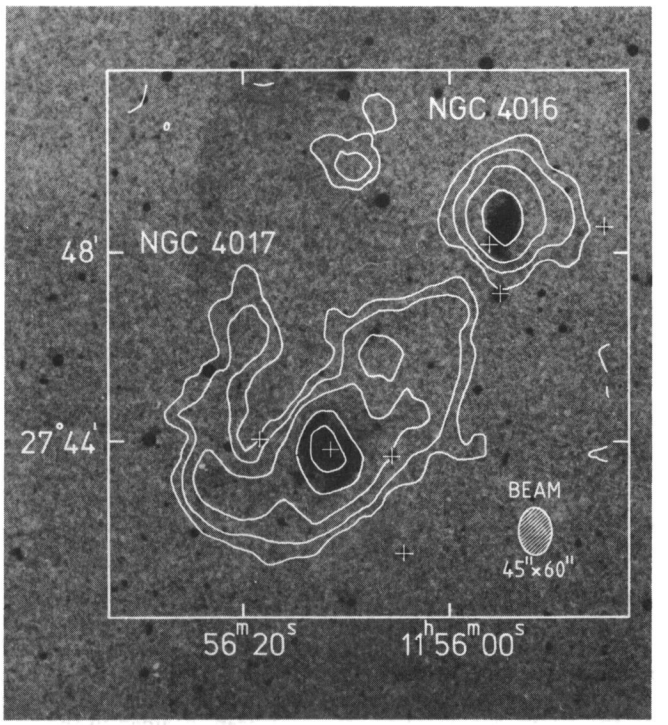

FIGURE 15. — Distribution of H1 in NGC 4016 and NGC 4017. Contours shown are 1.0, 2.1, 4.1, 8.3, and 12.4 × 10^{20} atoms/cm^2. The lowest contour corresponds approximately to a 2.5 σ noise level.

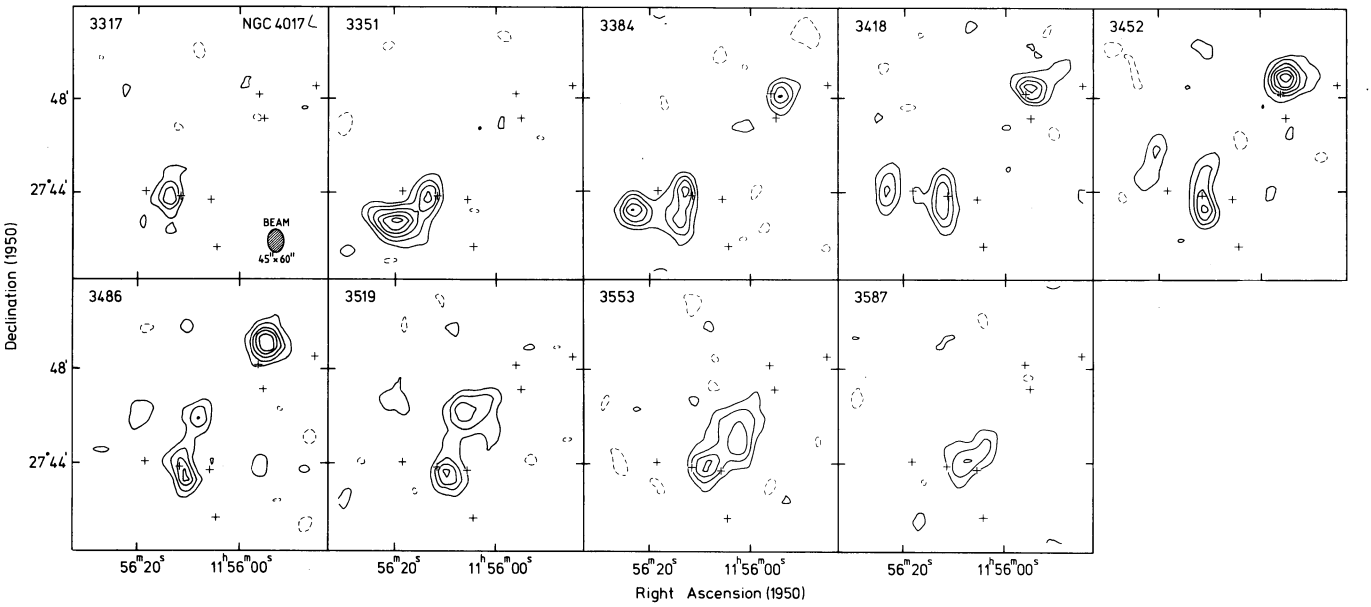

FIGURE 16. — Channel maps for the field around NGC 4016 and NGC 4017. The heliocentric radial velocity is indicated in the upper left corner of each panel. Only every other channel map is shown. Contours are − 1.0, 1.0, 2.1, 3.1, 4.2, 5.2, and 6.3 K brightness temperature. The lowest contour corresponds to a 2 σ noise level.

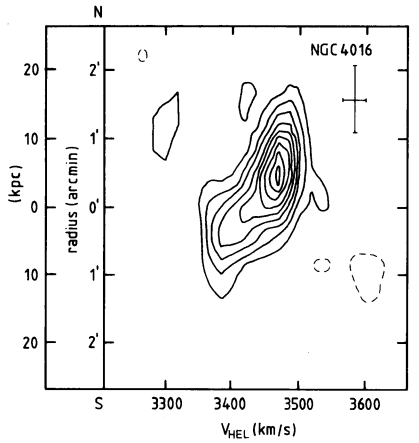

FIGURE 17. — Position-velocity plot along the major axis of NGC 4016, with an adopted position angle of 177°. Contours are − 0.9, 0.9, 1.9, 2.8, 3.7, 4.7, 5.6, 6.5, 7.4, and 8.4 K brightness temperature. The lowest contour (0.9 K) corresponds to a 1.8 σ noise level. The resolution in velocity and in space is indicated by the cross.

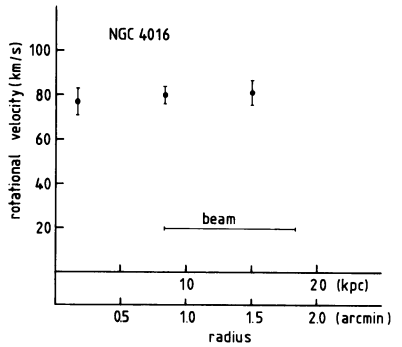

FIGURE 18. — Rotation curve of NGC 4016, determined from figure 17, and corrected for 60° inclination.

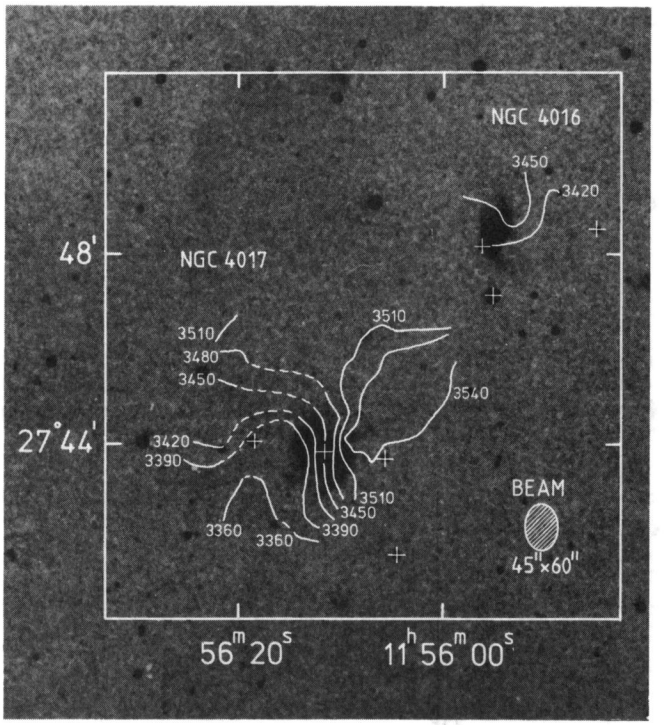

FIGURE 19. — Velocity field of NGC 4016 and NGC 4017. Contours are labelled by their corresponding heliocentric velocities. The dashed parts are not observed but interpolated by hand. This plot serves as an indication of the kinematics within the double system, but is not used in the actual analysis because of the presence of resolution effects.

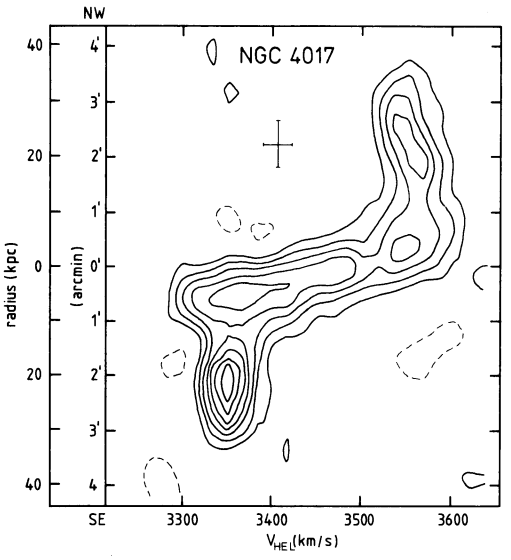

FIGURE 20. — Position-velocity plot of NGC 4017 along an axis through the centre and with a position angle of 126°. Contours are – 0.8, 0.8, 1.6, 2.4, 3.3, 4.1, 4.9, 5.7, and 6.5 K brightness temperature. The 0.8 K contour corresponds to a 1.6 σ noise level. The cross indicates the resolution in velocity and in space along the major axis.

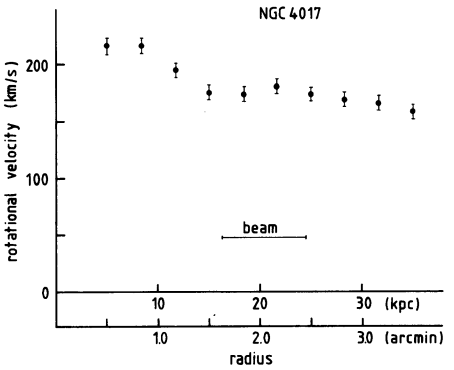

FIGURE 21. — Rotation curve of NGC 4017 assuming the axis in figure 20 to be the major axis of this galaxy. Velocities have been corrected for 45° inclination. The error bars do not include uncertainties in the adopted inclination angle.

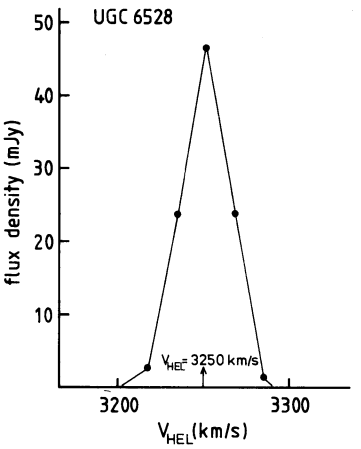

FIGURE 23. — Global profile of UGC 6528. The shape is equal to the instrumental velocity profile after Hanning smoothing, suggesting a small range in radial velocities centred at 3250 km/s.

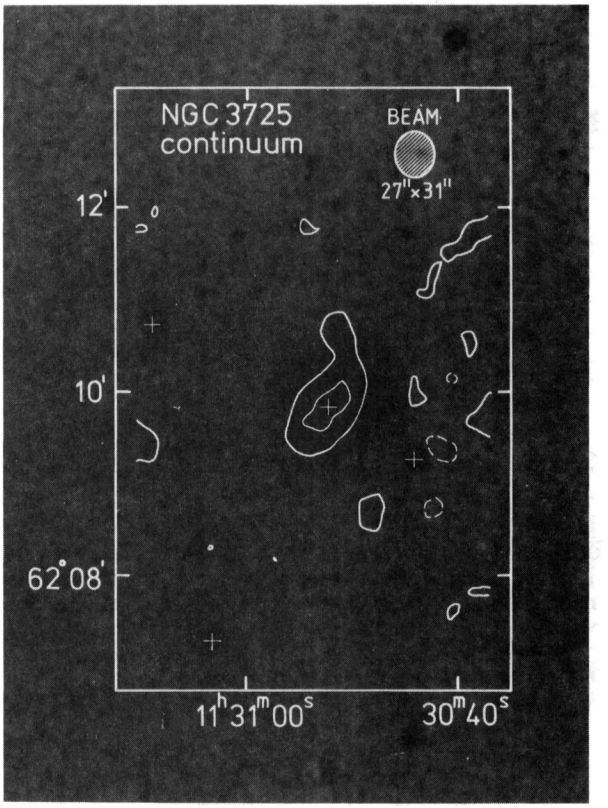

FIGURE 22. — Continuum map of NGC 3725 at 1405 MHz. The central cross indicates the optical position of NGC 3725. Contours are – 1.1, 1.1, and 2.2 mJy/beam area. The lowest contour corresponds to a 2 σ noise level, the total flux density is 9 ± 2 mJy.

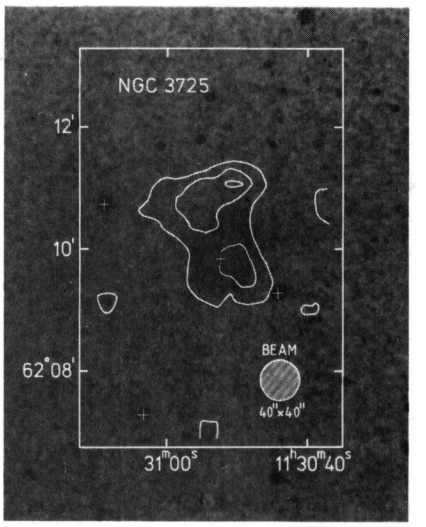

FIGURE 24. — HI map of NGC 3725. Contours shown are 1.4, 2.9, and 4.3 × 10^{20} atoms/cm^2. The lowest contour is approximately the 2 σ rms noise level.

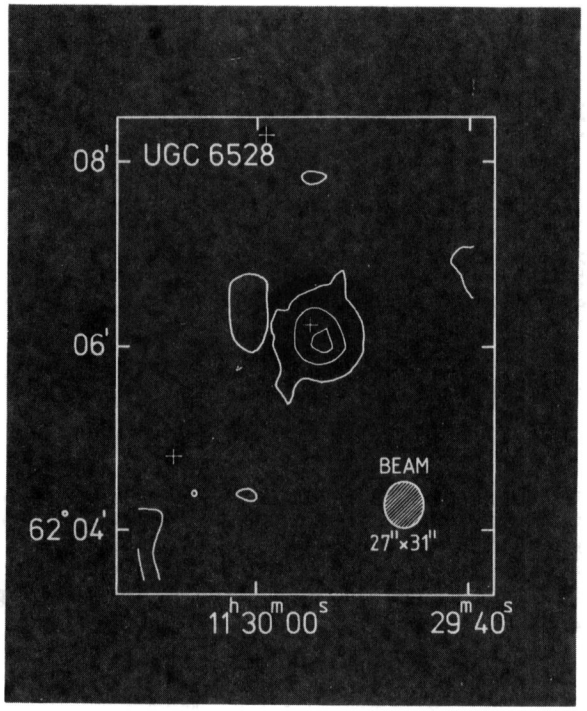

FIGURE 25. — HI map of UGC 6528, contours are 2.3, 4.6, and 6.8 × 10^{20} atoms/cm^2, where the lowest contour corresponds to a 2 σ noise level.

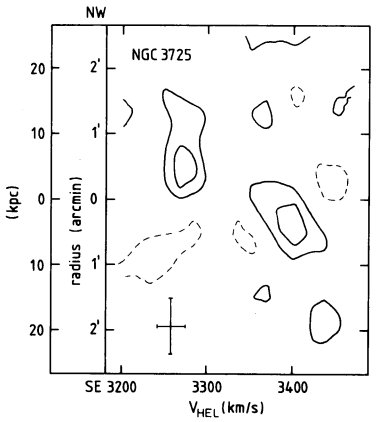

FIGURE 26. — Position-velocity plot of NGC 3725 through the optical central position (Table IV) and with a major axis position angle of 153°. Contours are – 2.2, 2.2 (1.5 σ rms noise), and 4.4 K brightness temperature.

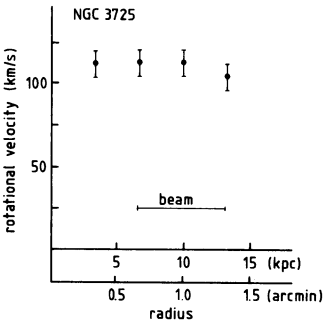

FIGURE 27. — Rotation curve of NGC 3725 determined from figure 26. The relatively high errors arise mainly from the noisy velocity profiles.

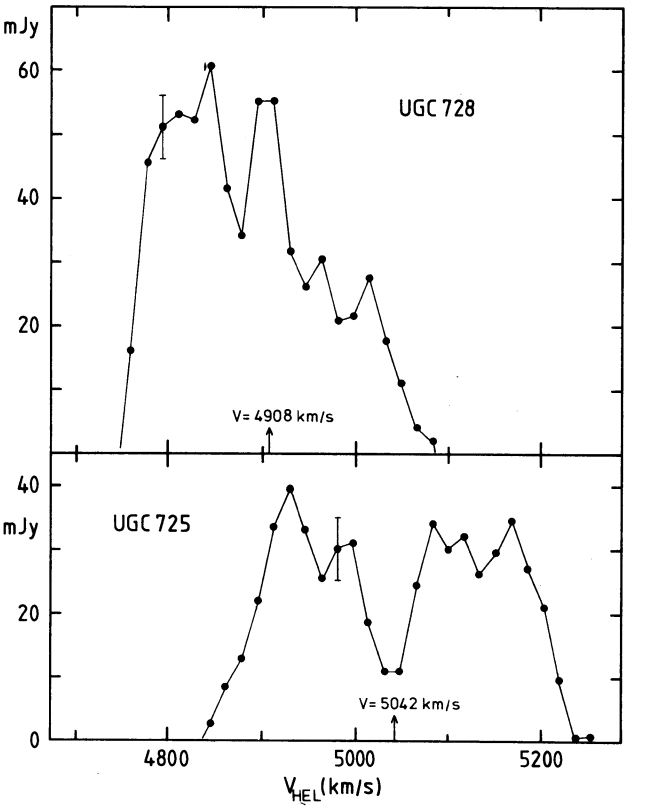

FIGURE 28. — Global profiles of UGC 725 and UGC 728 on the same velocity axis. Flux densities have been corrected for primary beam attenuation ; preliminary systemic velocities, determined from the profiles, are indicated.

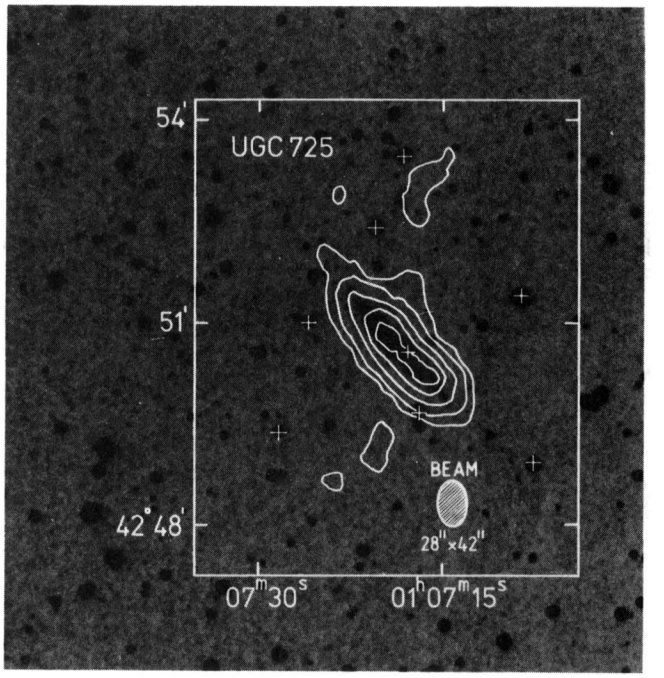

FIGURE 29. — HI map of UGC 725. Contours shown are 2.1, 4.1, 8.3, 12.4, and 16.5 × 10^{20} atoms/cm^2. The lowest contour of 2.1 × 10^{20} atoms/cm^2 corresponds approximately to a 2.5 σ detection level. The central cross indicates the adopted optical centre.

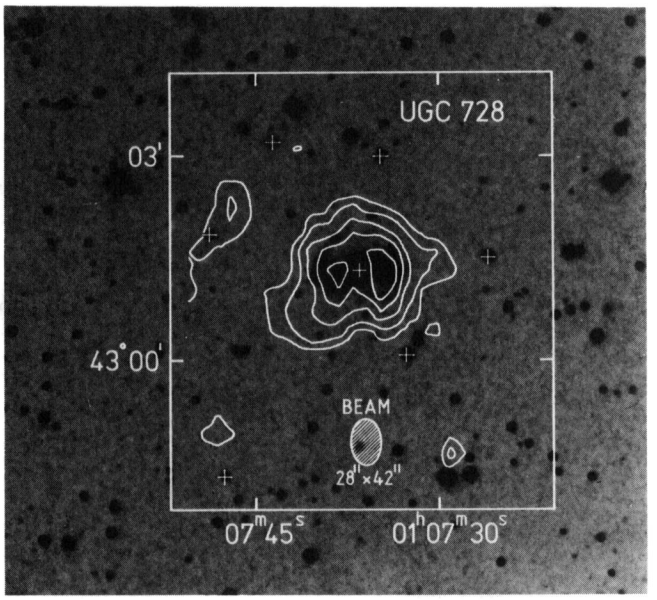

FIGURE 30. — HI map of UGC 728. Contours shown are 2.1, 4.1, 8.3, 12.4, and 16.5 × 10^{20} atoms/cm^2. The lowest contour corresponds approximately to a 2.5 σ detection level. The central cross indicates the adopted optical centre.

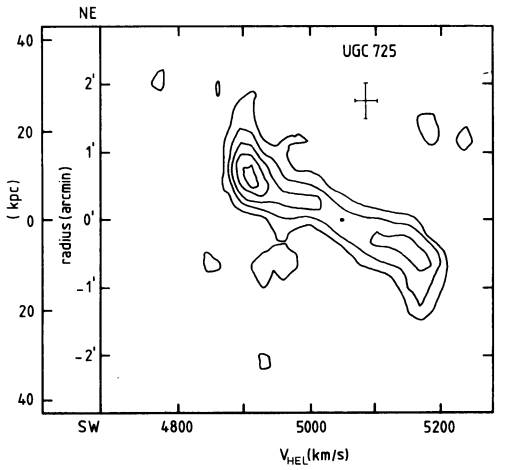

FIGURE 31. — Position-velocity plot of UGC 725 along the major axis, defined by the optical centre and a position angle of 43°. The contour values are − 2.0 (dashed), 2.0, 4.0, 6.0, 8.0, and 10.0 K brightness temperature. The 2.0 K contour corresponds to a 2.2 σ noise level. The cross indicates the resolution in velocity and in space along the major axis.

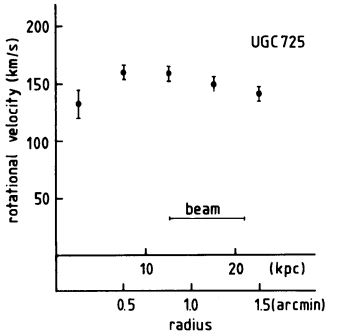

FIGURE 32. — Rotation curve of UGC 725, determined from figure 31. Velocities are corrected for 79° inclination.

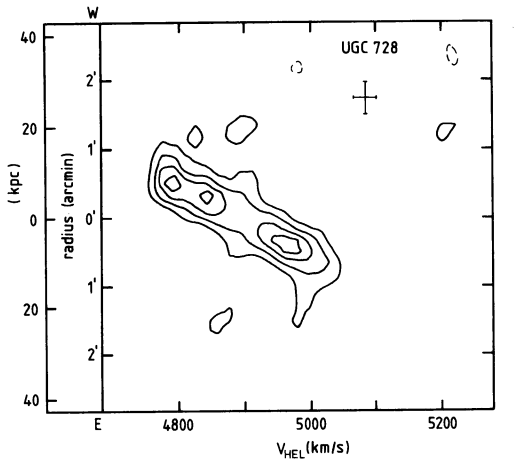

FIGURE 33. — Position-velocity plot along the major axis of UGC 728. This major axis is defined by the optical centre and a position angle of 103°. Contours are − 2.0 (dashed), 2.0, 4.0, 6.0, and 8.0 K brightness temperature ; the lowest contour lies at a 2.2 σ noise level. The resolution in velocity and in space along the major axis is indicated by the cross.

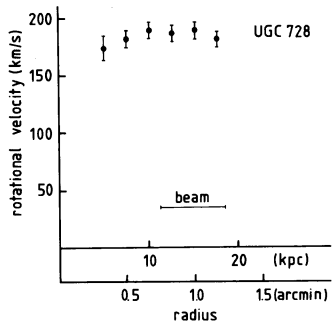

FIGURE 34. — Rotation curve of UGC 728, determined from the position-velocity plot in figure 27, and corrected for 45° inclination. The error bars do not include uncertainties arising from the imprecise inclination.

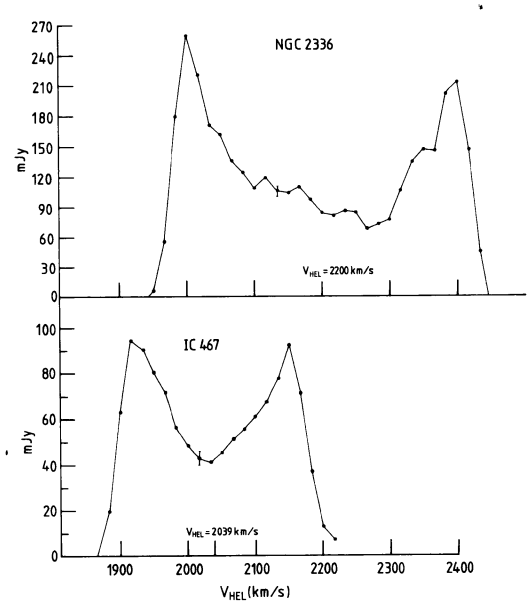

FIGURE 35. — Global HI profiles of NGC 2336 and IC 467 on a common velocity axis. Preliminary systemic velocities, derived from the profiles, are indicated. Flux densities have been corrected for primary beam attenuation.

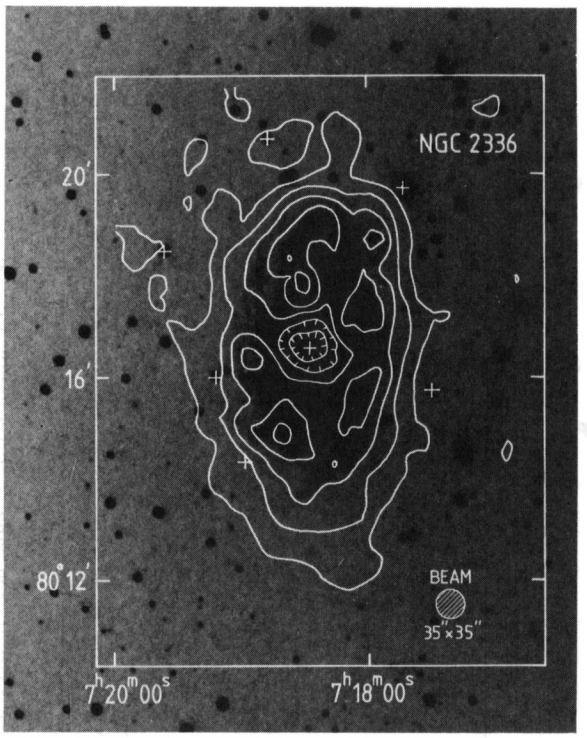

FIGURE 36. — HI map of NGC 2336. Contours shown are 1.5, 4.6, 7.7, 10.7, and 13.8 × 10^{20} atoms/cm^2. The lowest contour corresponds approximately to a 3 σ noise level. Note the lack of hydrogen at the centre ; the cross indicates the position of the optical centre.

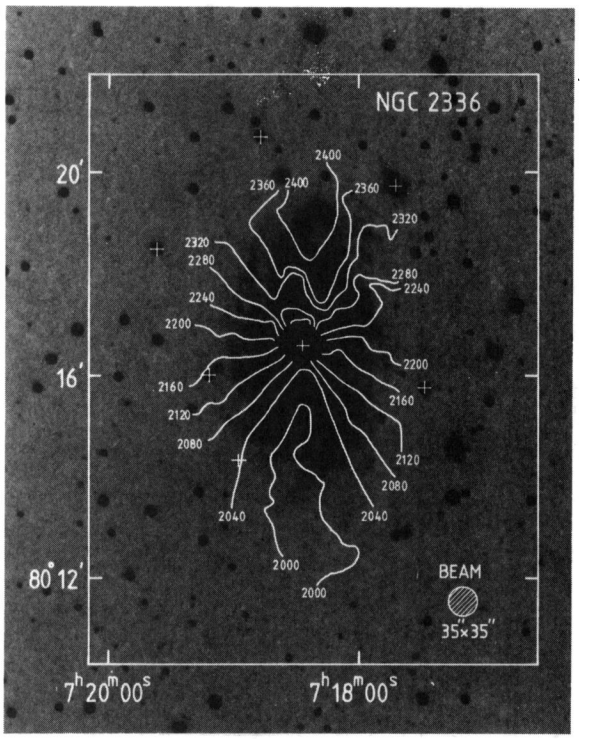

FIGURE 39. — Velocity field of NGC 2336. The isovelocity lines are labelled by their corresponding heliocentric velocities.

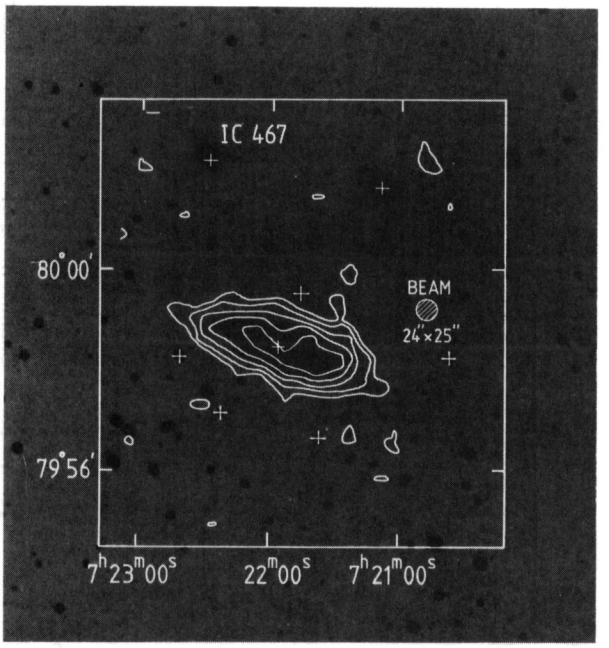

FIGURE 37. — HI map of IC 467. Contours shown are 1.8, 3.7, 7.4, 11.1, and 14.8 × 10^{20} atoms/cm^2. The lowest contour corresponds approximately to a 2.5 σ noise level.

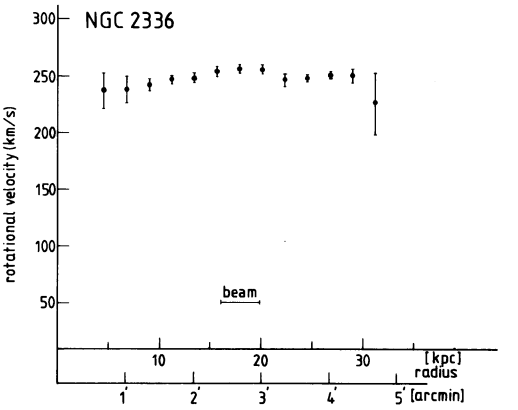

FIGURE 40. — Rotation curve of NGC 2336, determined from the velocity field in figure 39. The rotational velocities are corrected for an inclination angle of 59°.

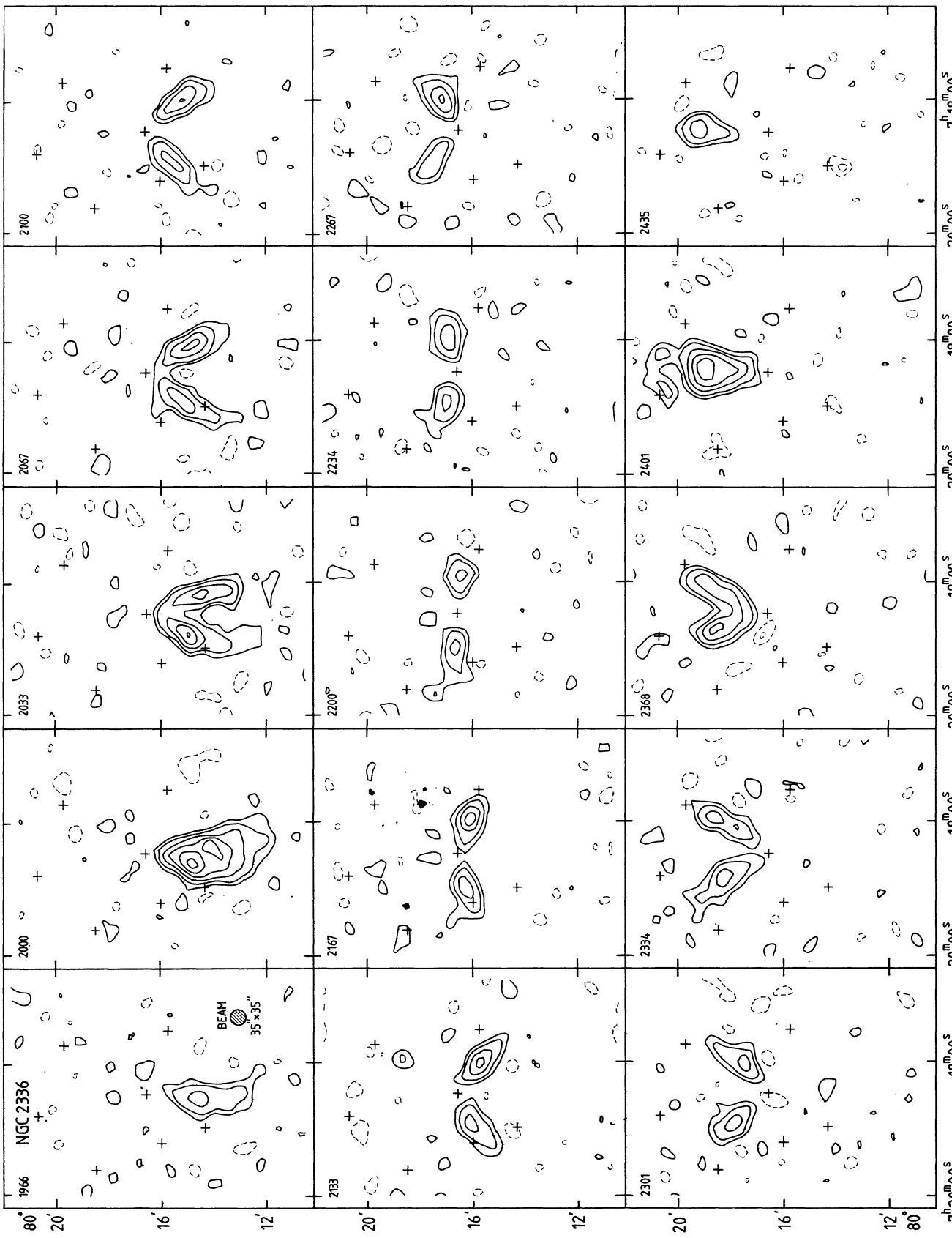

FIGURE 38. — Channel maps of NGC 2336. Heliocentric velocities are given in the upper left of each panel. Crosses are the same as in figure 36. Contours are − 2.0, − 1.0, 1.0, 2.0, 4.0, 6.0, 8.0, and 10.0 K brightness temperature. Negative contours are dashed. The lowest contour (1.0 K) corresponds to a 2.2 σ noise level.

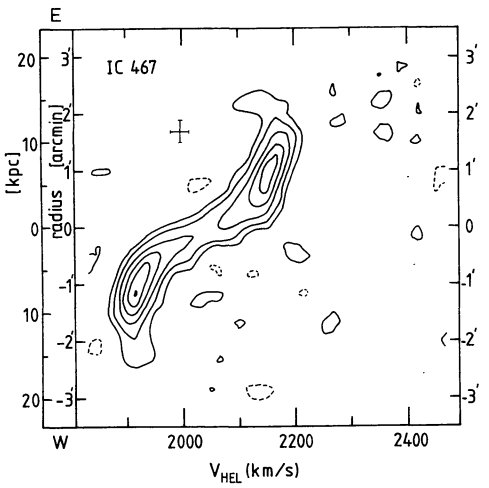

FIGURE 41. — Position-velocity plot of IC 467 along the major axis, defined by the optical centre and a position angle of 70°. The cross indicates the resolution in velocity and in space along the major axis. The contour values are − 1.6 (dashed), 1.6, 3.2, 6.5, 9.7, 12.9, and 16.2 K brightness temperature. The lowest contour (1.6 K) corresponds to a 2 σ noise level.

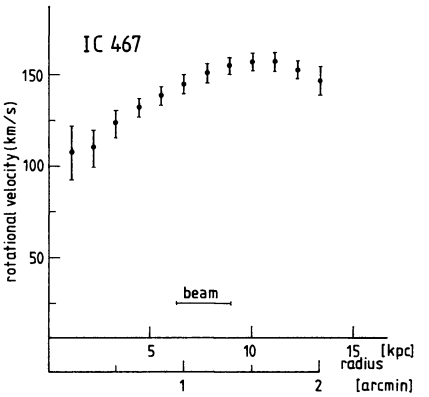

FIGURE 42. — Rotation curve of IC 467 as determined from figure 41, and corrected for 69° inclination.